DR. JOAQUIN ORTEGO (Orcid ID : 0000-0003-2709-429X)

Article type : Original Article

Geographic isolation versus dispersal: Relictual alpine grasshoppers support a model of interglacial diversification with limited hybridization

Joaquín Ortego[1] and L. Lacey Knowles[2]

[1]Department of Integrative Ecology, Estación Biológica de Doñana (EBD-CSIC), Avda. Américo Vespucio 26, E-41092 Seville, Spain

[2]Department of Ecology and Evolutionary Biology, University of Michigan, Ann Arbor, MI, USA

Author for correspondence:
Joaquín Ortego
Estación Biológica de Doñana, EBD-CSIC,
Avda. Américo Vespucio 26, E-41092 Seville, Spain
E-mail: joaquin.ortego@csic.es
Phone: +34 954 232 340

Running title: Genetic cohesiveness in alpine grasshoppers**Abstract**

Alpine biotas are paradigmatic of the countervailing roles of geographic isolation and dispersal during diversification. In temperate regions, repeated distributional shifts driven by Pleistocene climatic oscillations produced both recurrent pulses of population fragmentation and opportunities for gene flow during range expansions. Here, we test whether a model of divergence in isolation versus with gene flow is more likely in the diversification of flightless alpine grasshoppers of the genus *Podisma* from the Iberian Peninsula. The answer to this question also can provide key insights about the pace of evolution. Specifically, if the data fit a divergence in isolation model, it suggests rapid evolution of reproductive isolation. Genomic data confirm a Pleistocene origin of the species complex and multiple analytical approaches revealed limited asymmetric historical hybridization between two taxa. Genomic-based demographic reconstructions, spatial patterns of genetic structure and range shifts inferred from palaeodistribution modelling suggest severe range contraction accompanied by declines in effective population sizes during interglacials (i.e., contemporary populations confined to sky islands are relicts) and expansions during the coldest stages of the Pleistocene in each taxon. Although limited hybridization during secondary contact leads to phylogenetic uncertainty if gene flow is not accommodated when estimating evolutionary relationships, all species exhibit strong genetic cohesiveness. Our study lends support to the notion that the accumulation of incipient differences during periods of isolation were sufficient to lead to lineage persistence, but also that the demographic changes, dispersal constraints, and spatial distribution of the sky islands themselves mediated species diversification in temperate alpine biotas.

KEYWORDS distributional shifts, genetic cohesiveness, hybridization, introgression, Pleistocene, reticulate evolution, speciation

1. INTRODUCTION

The opportunities for divergence in isolation, but also the counteracting effects of gene flow during periods of secondary contact, are quintessential processes of Pleistocene speciation in alpine and montane biotas from temperate regions (Hewitt, 2000). Isolation of populations in glacial (Carstens & Knowles, 2007) or interglacial

(Bennett & Provan, 2008) refugia during the climatic oscillations of the Pleistocene is likely to have exposed them to different selective regimes and increased genetic drift, which ultimately are hypothesized to have promoted divergence and speciation (Hewitt, 1996; Stewart et al., 2010). Conversely, latitudinal displacements to or from glacial refugia and down-slope movements towards lower elevation areas during ice ages may contribute to geographical contact of gene pools that had remained isolated over extended periods of time (Knowles & Massatti, 2017; Maier et al., 2019; Tonzo et al., 2021). If incipient speciation during geographic isolation is not accompanied by effective reproductive isolation, secondary contact will lead to post-divergence gene flow (Hewitt, 2000). Depending on the permeability to gene exchange between previously allopatric lineages, the consequences of such process will range from speciation reversal (e.g., Maier et al., 2019) to different levels of introgressive hybridization (e.g., Melo-Ferreira et al., 2005). For these reasons, Pleistocene glacial-interglacial cycles are hypothesized to have acted both as "species pumps" and as "melting pots", creating opportunity for divergence and gene exchange across different stages along the continuum of speciation (April et al., 2013; Ebdon et al., 2021; Haffer, 1969; Hewitt, 1996, 2000; Knowles, 2001; Petit et al., 2003). Climate oscillations during the Quaternary are thus expected to have promoted reticulate speciation in many organism groups, rather than a strictly bifurcating evolutionary history of species divergence (Nevado et al., 2018; Thom et al., 2018).

An accurate reconstruction of the history of species divergence is a prerequisite for inferring the tempo and mode of speciation and testing alternative biogeographic and macro-evolutionary hypotheses regarding the processes underlying observed patterns of biological diversity (Nylander et al., 2008; Rangel et al., 2015; Tariel et al., 2016). However, the phylogenetic relationships of recently diverged species can be obscured by unresolved nodes (i.e., polytomies) (e.g., Kutschera et al., 2014; Takahashi et al., 2014). Phylogenetic uncertainties are frequently a consequence of incomplete lineage sorting (ILS) of ancestral polymorphism (Maddison & Knowles, 2006) and/or deviations from strictly bifurcating lineages due to horizontal gene transfer, hybrid speciation or introgression (Mallet et al., 2016; McBreen & Lockhart, 2006). Identifying the causes of phylogenetic conflict (i.e., reticulation versus ILS) is essential for distinguishing among alternative evolutionary pathways (e.g., de Manuel et al., 2016;

Schrago & Seuánez, 2019; Thom et al., 2018), which can ultimately provide key insights about the pace of speciation (Rosindell et al., 2010; Sukumaran & Knowles, 2017). However, this task is more daunting in recent Pleistocene radiations in which species may have weak reproductive barriers and short inter-speciation times that often co-occur with secondary introgression (i.e., post-divergence gene flow) (Nevado et al., 2018; Wen et al., 2016). In the last decade, increased capacity to generate large genomic datasets in non-model organisms has been critical to overcoming statistical uncertainties contributed by limited genetic information. This has also driven the development of numerous analytical approaches aimed at resolving gene tree discordances and detecting admixture (reviewed in Payseur & Rieseberg, 2016). Thanks to these analytical advances, we can now test speciation hypotheses that depart from models of divergence in strict isolation, which is key to considering whether introgressive hybridization is a component of the evolutionary portrait of diversification (e.g., de Manuel et al., 2016; Thom et al., 2018). However, given the assumptions and limitations inherent to each available approach, corroboration across multiple lines of evidence for complex histories of diversification is recommended (for details, see Payseur & Rieseberg, 2016).

Here, we use genomic data to evaluate the countervailing effects of dispersal and isolation on the speciation process and determine whether population isolation driven by Pleistocene glacial cycles triggered the necessary mechanisms for long-lasting genetic cohesion of lineages or if, on the contrary, extensive gene flow during periods of secondary contact have impaired their persistence and the formation of new species (Dynesius & Jansson, 2014). Specifically, we apply an integration of multiple approaches to unravel a Pleistocene diversification history of alpine grasshoppers of the genus *Podisma* from the Iberian Peninsula (Orthoptera: Acrididae) (Morales-Agacino, 1951). As the southernmost distributional limit of the genus, the region hosts three species distributed in allopatry across different mountain ranges (Cigliano et al., 2021; Figure 1). The three taxa are distributed at elevations >1200 m, restricted to montane and alpine open habitats dominated by low grasslands and dwarf shrub formations (e.g., *Juniperus* sp., *Vaccinium* sp., and *Rhododendron* sp.), which are interspersed with patches of bare ground and rocks (Presa et al., 2016a, b; Zuna-Kratky et al., 2016). As such, their contemporary populations are extremely

fragmented across sky islands of suitable habitat embedded in an inhospitable matrix characteristic of the Mediterranean climate (Cigliano et al., 2021; Presa et al., 2016a, b; Zuna-Kratky et al., 2016). There are no clear phenological differences among the taxa; the three species are univoltine (i.e., a single generation per year) with adult populations peaking in July-August (Morales-Agacino, 1951; Zuna-Kratky et al., 2016; Joaquín Ortego, pers. obs.). They are very similar in external appearance and are flightless, with *P. pedestris* and *P. carpetana* being micropterus and *P. cantabricae* apterous, although rare macropterous (i.e., fully-winged) forms have occasionally been described in *P. pedestris* (Lemonnier-Darcemont & Darcemont, 2004; Morales-Agacino, 1951). Capture-mark-release-recapture studies on *P. pedestris* indicate that these taxa exhibit very low dispersal capacities and a marked philopatric behavior (Barton & Hewitt, 1981, 1982; Mason et al., 1995). Due to this limited dispersal ability and strict habitat requirements, we hypothesize that recurrent pulses of population expansions and contractions during Pleistocene glacial cycles have contributed to genetic isolation and speciation, but that the shifting distributions also generated repeated opportunities for post-divergence gene flow (e.g., Barton, 1980; Keller et al., 2008). To accommodate an evolutionary history that may depart from assumptions of divergence in isolation and to gain insights into the processes underlying speciation that includes the possibility of post-divergence gene flow, we integrate a comprehensive suite of phylogenomic and population genomic approaches with paleoclimate-based reconstructions of species distributions. Specifically, we apply the multispecies coalescent (MSC) model to infer phylogenetic relationships among taxa and identify nodes with potential conflict that might be indicative of either ILS or reticulation. Then, we perform phylogenetic tests to distinguish ILS from introgression and use a model-based approach to evaluate alternative scenarios of post-divergence gene flow or lack thereof. Using environmental niche modelling and paleoclimate-based reconstructions of species distributions, we infer range shifts during glacial/interglacial periods in each species and use this framework to determine which expectations in terms of population fragmentation and secondary contact are most probable given species divergence, past demography, and introgressive hybridization estimated based on the genomic data.

2. MATERIALS AND METHODS

2.1. Population sampling

Occurrence records from the literature were used to design sampling and guide collection of specimens from populations representative of the distribution range of each of the three *Podisma* taxa from the Iberian Peninsula: *Podisma pedestris* (Linnaeus, 1758), *Podisma carpetana* Bolívar, 1898, and *Podisma cantabricae* Morales-Agacino, 1950 (Figure 1; details given in Table S1). Seven specimens of *Cophopodisma pyrenaea* (Fischer, 1853) (tribe Podismini; Cigliano et al., 2021) were used as an outgroup in phylogenomic analyses and ABBA/BABA tests (Table S1). Spatial coordinates were recorded using a Global Positioning System (GPS) and whole specimens were preserved at -20 °C in 1,500 µL of 96% ethanol until needed for genomic analyses.

2.2. Genomic library preparation and processing

We used NucleoSpin Tissue (Macherey-Nagel, Düren, Germany) kits to extract and purify DNA from a hind leg of each individual. We processed genomic DNA into one genomic library using the double-digestion restriction-site associated DNA sequencing procedure (ddRAD-seq) described in Peterson et al*.,* (2012). In brief, we digested DNA with the restriction enzymes MseI and EcoRI (New England Biolabs, Ipswich, MA, USA) and ligated Illumina adaptors including unique 7-bp barcodes to the digested fragments of each individual. We pooled ligation products and size-selected 475-580 bp fragments with a Pippin Prep machine (Sage Science, Beverly, MA, USA), amplified the fragments by PCR with 12 cycles using the iProofTM High-Fidelity DNA Polymerase (BIO-RAD, Veenendaal, The Netherlands), and sequenced the library in a single-read 150-bp lane on an Illumina HiSeq2500 platform at The Centre for Applied Genomics (Toronto, ON, Canada). Raw sequences were demultiplexed and preprocessed using STACKS v. 1.35 (Catchen et al., 2013) and assembled using PYRAD v. 3.0.66 (Eaton, 2014); see Supplementary Methods S1 for details on sequence assembling and data filtering. The choice of different filtering and assembling thresholds had a little impact on the obtained inferences (see Results section; e.g., Eaton, 2014; Ortego et al., 2018). For this reason, unless otherwise indicated, all downstream analyses were performed

using datasets of unlinked SNPs (i.e., using a single SNP per RAD locus) obtained with PYRAD considering a clustering threshold of sequence similarity of 0.85 (W_{clust} = 0.85) and excluding loci that were not present in at least 20 individuals (*minCov* = 20). We used the option *relatedness2* in VCFTOOLS to calculate the relatedness among all pairs of genotyped individuals and to exclude the possibility that we had sampled close relatives within each study population (Danecek et al., 2011; Manichaikul et al., 2010).

2.3. Quantifying genetic structure

We analyzed population genetic structure and admixture using the Bayesian Markov chain Monte Carlo clustering method implemented in the program STRUCTURE v. 2.3.3 (Pritchard et al., 2000). We conducted STRUCTURE analyses hierarchically, initially analysing data from all populations and species jointly and, subsequently, running independent analyses for subsets of populations assigned to the same genetic cluster in the previous hierarchical level analysis (Janes et al., 2017; Pritchard et al., 2000). We ran STRUCTURE using a random subset of 10,000 SNPs with 200,000 MCMC cycles after a burn-in step of 100,000 iterations, and assuming correlated allele frequencies and admixture (Pritchard et al., 2000). We performed 15 independent runs for each value of *K* genetic clusters, where *K* ranged from 1 to *n* + 1 for each dataset of *n* populations, to estimate the most probable number of clusters. We retained the ten runs with the highest likelihood for each *K*-value. As recommended by Gilbert et al. (2012) and Janes et al. (2017), we used two statistics to interpret the number of genetic clusters (*K*) that best describes our data: log probabilities of Pr(X|*K*) (Pritchard et al., 2000) and Δ*K* (Evanno et al., 2005). These statistics were calculated as implemented in STRUCTURE HARVESTER (Earl & vonHoldt, 2012). We used CLUMPP v. 1.1.2 and the Greedy algorithm to align multiple runs of STRUCTURE for the same *K*-value (Jakobsson & Rosenberg, 2007) and DISTRUCT v. 1.1 (Rosenberg, 2004) to visualize the individual`s probabilities of genetic cluster membership as bar plots. Complementary to Bayesian clustering analyses, we performed principal component analyses (PCA) as implemented in the R v. 4.0.3 (R Core Team, 2021) package *adegenet* (Jombart, 2008). Before running the PCAs, we replaced missing data by the mean frequency of the corresponding allele estimated across all samples (Jombart, 2008).

2.4. Phylogenomic inference

We estimated species trees using two coalescent-based methods: SNAPP v. 1.3 (Bryant et al., 2012) as implemented in BEAST v. 2.4.1 (Bouckaert et al., 2014) and SVDQUARTETS (Chifman & Kubatko, 2014) as implemented in PAUP* v. 4.0a152 (Swofford, 2002).

SNAPP – For the SNAPP analyses, we ran two independent replicates of >2 million generations sampled every 1,000 steps (i.e., >2,000 retained genealogies), removing 10% of trees as burn-in. Stationarity and convergence of the chains was assessed with TRACER v. 1.4 to confirm that effective sample sizes (ESS) for all parameters were > 200. We combined tree and log files for replicated runs using LOGCOMBINER v. 2.4.1 and used TREEANNOTATOR v. 1.8.3 to obtain maximum clade credibility trees and TREESETANALYSER v. 2.4.1 to identify species trees that were contained in the 95% highest posterior density (HPD) set. Pilot analyses with different values of the shape (α) and inverse scale (β) parameters of the gamma prior distribution (α= 2, β= 200; α= 2, β= 2,000; α= 2, β= 20, 000) for the population size parameter (θ), leaving default settings for all other parameters, yielded the same topology (not shown); only results for the intermediate prior for theta (α= 2, β= 2,000) are presented. The full set of trees was displayed with DENSITREE v. 2.2.1 (Bouckaert, 2010), which is expected to show fuzziness in parts of the tree due to gene flow or other causes of phylogenetic conflict. Due to large computational demands of SNAPP, we only included three individuals per population for the ingroup.

SVDQUARTETS – We ran SVDQUARTETS to estimate the evolutionary relationships of populations from each species (i.e., a population/species tree; Knowles & Carstens, 2007) by evaluating 10,000 random quartets from the dataset; uncertainty in relationships was quantified using 100 bootstrapping replicates. Given the low computational burden of SVDQUARTETS in comparison with SNAPP, we analyzed six SNP matrices obtained by setting different values of clustering thresholds (W_{clust} = 0.85 and 0.90) and minimum taxon coverage for a locus (*minCov* = 10, 20 and 30) (see Methods S1). This allowed us to assess the impact of different proportions of missing data and number of loci on the estimated topology and patterns of branch support (Huang & Knowles, 2016; Noguerales et al., 2018; Takahashi et al., 2014).

2.5. Analyses of introgression

Although phylogenetic analyses tended to support *P. carpetana* and *P. cantabricae* as sister taxa, the relationships among the three species often remained unresolved (see Results section). To determine the role of incomplete lineage sorting versus introgression in explaining such conflicting phylogenetic relationships, we tested the possibility of post-divergence gene flow using a comprehensive suite of approaches detailed below. Note that these analyses (with the exception of PHYLONETWORKS) were carried out sequentially using one representative population per species, and then testing all population combinations, because intraspecific population structure (see Figure 1) can confound analyses that assume panmixia within species.

Phylogenetic networks – We used Species Networks applying Quartets (SNAQ) implemented in PHYLONETWORKS (Solís-Lemus et al., 2017) to determine whether a strictly bifurcating phylogenetic tree (i.e., no hybridization) or a phylogenetic network (i.e., one or more introgression events) better explains the evolutionary history of *Podisma* grasshoppers. SNAQ performs maximum pseudo-likelihood estimation of phylogenetic networks using the multispecies coalescent model and quartet-based concordance analyses (Solís-Lemus et al., 2017) to infer the most likely network, depict the major phylogenetic topology ("major edge") and past introgression events ("minor edges"), and calculate γ, the vector of inheritance probabilities describing the proportion of genes inherited by a hybrid node from one of its parents (Solís-Lemus et al., 2017). The MAGNET v. 0.1.5 pipeline (J.C. Bagley, http://github.com/justincbagley/MAGNET) was used to split each locus contained in the PYRAD output file '.gphocs' into a separate phylip-formatted alignment file and run RAXML v. 8.2.12 (Stamatakis, 2014) to infer a maximum-likelihood (ML) gene tree for each locus with the GTR+GAMMA model and 100 bootstrap replicates. Prior to obtaining gene trees, we applied TRIMAL v. 1.2 (Capella-Gutiérrez et al., 2009) to our phylip dataset to filter out loci with a high mean percentage of identity (>0.95) across the multisequence alignment and retain only those (1,447 loci) that are most informative (Bernardes et al., 2007). We used these gene trees and PHYLONETWORKS to estimate quartet concordance factors (CFs), defined as the proportion of genes that

support each possible relationship between each set of four taxa. We used the topology obtained with SNAPP as a starting tree and estimated the best phylogenetic network testing a varying number of reticulation events (*h* from 0 to 5), each optimized with 10 independent runs. The optimal number of reticulation events was chosen using a heuristic approach by plotting negative pseudo-likelihood scores against *h*-values, as recommended by the authors (Solís-Lemus et al., 2017).

D-statistics – We used four-taxon ABBA/BABA tests based on the *D*-statistic to test for introgression as an explanation for conflicting phylogenetic relationships (Durand et al., 2011). Briefly, for the sister species P1 and P2 (i.e., *P. cantabricae* and *P. carpetana*, respectively), which diverged from a common ancestor with P3 (i.e., *P. pedestris)*, and the outgroup O (i.e., *C. pyrenaea*), the *D*-statistic is used to test the null hypothesis of no introgression ($D = 0$) between P3 and P1 or P2. *D*-values significantly different from zero indicate gene flow between P1 and P3 ($D < 0$) or between P2 and P3 ($D > 0$). We performed ABBA/BABA tests in PYRAD and used 1,000 bootstrap replicates to obtain the standard deviation of the *D*-statistic and significance levels (Eaton & Ree, 2013). We ran ABBA/BABA tests sequentially for each of the six different species-population combinations (i.e., using each population as a representative for a species). Only populations with ≥ 6 genotyped individuals were considered for these analyses (see Table S1). We ran these analyses using six different genetic datasets obtained by setting different clustering thresholds ($W_{clust} = 0.85$ and 0.90) and minimum taxon coverage for a given locus (*minCov* = 10, 20 and 30).

Population graphs – We analyzed the potential presence of introgression and determined the direction of gene flow using TREEMIX v. 1.12 (Pickrell & Pritchard, 2012). TREEMIX fits a population graph based on population allele frequencies and a Gaussian approximation to genetic drift, inferring patterns of splits and admixtures. We ran TREEMIX analyses considering the same six species-population combinations used for ABBA/BABA tests, assuming independence of all SNPs with a window size of one SNP ($k = 1$). Using an estimated maximum-likelihood tree rooted with the outgroup *C.*

313 *pyrenaea*, we tested a range of migration events (*m* from 0 to 4) and determined the
314 best fit model for the data by plotting Ln(likelihood) scores against *m*-values.
315
316 *Models of interspecific gene flow* – We used FASTSIMCOAL2 (Excoffier et al., 2013) to
317 evaluate the fit of the data to ten alternative divergence models that considered
318 different scenarios of interspecific gene flow (see Figure S1); the timing of gene flow
319 was modeled as a time interval, with an estimate for the time gene flow was initiated
320 ($T_{INTROG1}$) and the time that it ended ($T_{INTROG2}$; Figure S1). We estimated the composite
321 likelihood of the observed data (analyzing one SNP per locus) given a specified model
322 using the site frequency spectrum (SFS) and the simulation-based approach
323 implemented in FASTSIMCOAL2 (Excoffier et al., 2013). Separate analyses of one
324 population per species were performed considering six different species-population
325 combinations, as done for ABBA/BABA tests and TREEMIX analyses. Because invariable
326 sites were not included in the SFS, we fixed the effective population size for one
327 species (*P. cantabricae*) to enable the estimation of other parameters in FASTSIMCOAL2
328 (Excoffier et al., 2013); the fixed effective population size was calculated from the level
329 of nucleotide diversity ($\pi = 0.0005$) and the mutation rate per site per generation (2.8×10^{-9})
330 estimated for *Drosophila melanogaster* (Keightley et al., 2014), which is similar
331 to the spontaneous mutation rate estimated for the butterfly *Heliconius melpomene*
332 (2.9×10^{-9}; Keightley et al., 2015). To remove all missing data for the calculation of the
333 joint SFS (as required), each population group was downsampled to 5 individuals using
334 the *easySFS.py* script (I. Overcast, https://github.com/isaacovercast/easySFS).
335 Each model was run 100 replicated times considering 100,000-250,000
336 simulations for the calculation of the composite likelihood, 10-40 expectation-
337 conditional maximization (ECM) cycles, and a stopping criterion of 0.001 (Excoffier et
338 al., 2013). We used an information-theoretic model selection approach based on the
339 Akaike's information criterion (AIC) to determine the probability of each model given
340 the observed data (Burnham & Anderson, 2002). Specifically, AIC values for each
341 model were rescaled (ΔAIC) calculating the difference between the AIC value of each
342 model and the minimum AIC obtained among all competing models (i.e., the best
343 model has ΔAIC = 0; see Thome & Carsterns, 2016). Point estimates of the different
344 demographic parameters for the best supported model were selected from the run

with the highest maximum composite likelihood, with confidence intervals (based on the percentile method; e.g., de Manuel et al., 2016) calculated from 100 parametric bootstrap replicates of simulated SFS under the maximum composite likelihood parameter estimates (Excoffier et al., 2013).

2.6. Inference of past demographic history

We reconstructed the past demographic history from the site frequency spectrum (SFS) using the program STAIRWAY PLOT v. 2.1, which does not require whole-genome sequence data or reference genome information (Liu & Fu, 2015, 2020). We computed the SFS for each population as described in the previous section and ran STAIRWAY PLOT fitting a flexible multi-epoch demographic model, considering 1 generation per year (Barton & Hewitt, 1981), assuming a mutation rate of 2.8×10^{-9} per site per generation (Keightley et al., 2014), and performing 200 bootstrap replicates to estimate 95% confidence intervals.

2.7. Environmental niche modelling

We estimated environmental niche models (ENM) to (i) predict the geographic distribution of climatically suitable areas for the three species both in the present and during the last glacial maximum (LGM, 21 ka) and to (ii) determine if they support historical geographic contact among species (i.e., overlap of predicted distributions), which might explain observed patterns of genetic introgression (see Results section). We used the maximum entropy algorithm implemented in MAXENT v. 3.3.3 (Phillips et al., 2006; Phillips & Dudík, 2008), the 19 bioclimatic variables from the WORLDCLIM dataset (http://www.worldclim.org/) interpolated to 30-arcsec resolution (~1 km^2 cell size) (Hijmans et al., 2005), and species occurrence data, which included our own collections and records available in the literature and the Global Biodiversity Information Facility (GBIF.org, 06 February 2018, GBIF Occurrence Downloads; *P. pedestris*: https://doi.org/10.15468/dl.e78df8; *P. carpetana*: https://doi.org/10.15468/dl.jy1fiu; *P. cantabricae*: https://doi.org/10.15468/dl.ngt6yi). We mapped and examined all records to identify and exclude obvious geo-referencing errors and duplicate records (i.e., those falling within the same grid cell); this left final datasets of 5 entries for the narrow endemic *P. cantabricae*, 36 entries for *P.*

carpetana, and 34 entries for *P. pedestris*. Although the number of available records is small, particularly for the narrowly distributed *P. cantabricae*, similar sample sizes have been proven to be enough to develop ENMs with a good predictive power using MAXENT (e.g., Papes & Gaubert, 2007; van Proosdij, Sosef, Wieringa, & Raes, 2016; Wisz et al., 2008). We used the R package *ENMeval* (Muscarella et al., 2014) to conduct species-specific parameter tuning and determine the optimal feature class (FC) and regularization multiplier (RM) settings for MAXENT using a delete-one jackknife optimization approach, as recommended for small datasets (Muscarella et al., 2014; Shcheglovitova & Anderson, 2013). We tested a total of 248 models of varying complexity by combining a range of regularization multipliers (RM) (from 0 to 15 in increments of 0.5) with eight different feature classes (FC) combinations (L, LQ, LQP, H, T, LQH, LQHP, LQHPT, where L = linear, Q = quadratic, H = hinge, P = product and T = threshold) (Muscarella et al., 2014). Model performance was compared using the minimum training presence omission rate (OR_{MTP}) as the primary optimality criterion (to protect against overfitting) and the area under the curve of the receiver-operating characteristic plot on the testing data (AUC_{TEST}) as secondary criterion (to maximize the discriminatory ability of the model) (see Wachter et al., 2016). We selected model parameters (RM and FC) and the set of environmental variables retained in the final model following the multi-step approach detailed in González-Serna et al., (2019). To generate maps with predicted distributions during the LGM, we projected species-specific ENMs onto LGM bioclimatic conditions derived from the MIROC-ESM (Model of Interdisciplinary Research on Climate; Hasumi & Emori, 2004) and the CCSM4 (Community Climate System Model; Braconnot et al., 2007) general atmospheric circulation models. Climatically suitable areas for each species and time period were identified by converting the logistic outputs from MAXENT into binary maps using the maximum training sensitivity plus specificity (MTSS) threshold value for occurrence (Liu et al., 2005).

3. RESULTS

3.1. Genomic data

A total of 42,277,831 (mean ± SD = 3,019,845 ± 984,204 reads/individual), 58,328,181 (mean ± SD = 2,160,303 ± 929,130 reads/individual), 22,308,056 (mean ± SD = 3,186,865 ± 497,316 reads/individual), and 23,824,106 (mean ± SD = 3,403,443 ± 568,441 reads/individual) reads were obtained for *P. pedestris*, *P. carpetana*, *P. cantabricae*, and *C. pyrenaea*, respectively. The number of reads retained after the different quality filtering steps averaged 85% (Figure S2) and the final dataset contained 23,517 loci, of which 23,333 were variable and contained at least one SNP (mean number of SNPs per RAD locus = 9.49, excluding the outgroup) under a clustering threshold of sequence similarity of 0.85 (W_{clust} = 0.85) and discarding loci in less than 20 individuals (*minCov* = 20). All pairs of genotyped individuals had negative relatedness values (ranging from -6.56 to -0.09), which excludes the possibility that we had sampled close relatives (Manichaikul et al., 2010).

3.2. Quantifying genetic structure

For the STRUCTURE analyses, the LnPr(X|*K*) plateaued at *K* = 3 and Δ*K* peaked at the same *K*-value (Figure S3a), which corresponds to the three taxa, with no sign of genetic admixture among them (i.e., individual and population probabilities of membership = 1; Figure 1a). STRUCTURE analyses performed separately on *P. pedestris* and *P. carpetana* revealed a strong population genetic structure within each species (Figure 1a). Two genetic clusters inferred for *P. pedestris* (Figure S3b) group individuals by the two analyzed populations for this species (AUL and AIG), with no signs of genetic admixture (Figure 1a). For *P. carpetana*, the most likely number of clusters was *K* = 2 according to the Δ*K* criterion, but LnPr(X|*K*) steadily increases up to *K* = 4 (Figure S3c). These analyses reveal a north-south hierarchical genetic structure, with some signs of admixture restricted to some nearby populations from the Iberian System (DEM-URB and URB-MON; see Figure 1). Principal component analyses (PCA) separate well the three taxa and most populations within taxa, supporting the results from STRUCTURE (Figure S4).

3.3. Phylogenomic inference

The monophyly of all taxa and the same species relationships were estimated by both SNAPP and SVDQUARTETS (Figures 2 and S5). Phylogenetic relationships among species are

well supported with SNAPP (PP > 0.98; Figure 2a), but not with SVDQUARTETS (Figures 2b and S5), although the estimates from SVDQUARTETS are robust to different schemes of data filtering and assembling (Figure S5). The phylogenetic relationships among geographically proximate populations of *P. carpetana* were not well resolved by either SNAPP or SVDQUARTETS (Figure 2; see also Figure S5). In SNAPP, the three topologies contained in the 95% HPD tree set differed only in the population relationships inferred for *P. carpetana* (Table S2). These unresolved population relationships within *P. carpetana* are not unexpected given evidence of gene flow among nearby populations located in the same mountain range from STRUCTURE (Figure 1a) and PCA analyses (Figure S4).

3.4. Analyses of introgression

Phylogenetic networks – PHYLONETWORK analyses revealed that all models involving reticulation events ($h > 0$) fit our data better than models considering strict bifurcating trees ($h = 0$) (Figure S6). Negative pseudo-likelihood scores decrease sharply from $h = 0$ to $h = 2$ and remain unaltered or with a very small improvement for $h > 2$ (Figure S6), suggesting that the best-fitting phylogenetic model includes two introgression events. One inferred introgression event (γ_A) is from *P. pedestris* into *P. carpetana,* with ca. 11% of gene copies in the ancestor of *P. carpetana* traced to the ancestor of the two populations of *P. pedestris* (Figure 2c). The other inferred introgression event (γ_B) is from DEM to URB populations of *P. carpetana,* with ca. 48% of genetic material of population URB originated from DEM (Figure 2c), which is qualitatively similar to the results from STRUCTURE (Figure 1a). The backbone of the tree recovered with PHYLONETWORKS is consistent with those obtained with SNAPP and SVDQUARTETS, differing only in the phylogenetic relationships of some nearby populations of *P. carpetana* from the Iberian System (Figure 2).

D-statistics – A statistically significant excess of ABBA patterns ($D>0$) supports post-divergence gene flow between *P. pedestris* (P3) and *P. carpetana* (P2) (Table 1). This result holds irrespective of which population-species combinations were analyzed, or the data filtering and assembling scheme used in generating the dataset (Table S3).

Population graphs – TREEMIX analyses consistently support a single migration event (Figure S7) of directional gene flow from *P. pedestris* to *P. carpetana* (Figures 3 and S8).

Models of interspecific gene flow – FASTSIMCOAL2 analyses performed for all population-species combinations consistently show that the most supported scenario is one with asymmetrical gene flow from *P. pedestris* to *P. carpetana* (Figure 4; Model B in Table S4). Considering the 1-year generation time of these species (Barton & Hewitt, 1981), the split between *P. pedestris* and the two other taxa is estimated to have taken place ca. 638-992 ka ago, during the early-middle Pleistocene (Figure 4; Table S5). The split between *P. carpetana* and *P. cantabricae* is estimated as ca. 131-155 ka ago, during the middle Pleistocene (Figure 4; Table S5). Gene flow from *P. pedestris* to *P. carpetana* is inferred to have taken place during the middle-late Pleistocene, between ca. 108-147 ka and 87-120 ka ago (Figure 4; Table S5). It should be noted that estimates for the 95% confidence intervals for the oldest demographic parameters (θ_{ANC}, $\theta_{CAR\text{-}CAN}$, and T_{DIV1}) are much wider than those for more recent events (θ_{PED}, θ_{CAR}, T_{DIV2}, $T_{INTROG1}$, and $T_{INTROG2}$) (Figure 4; Table S5), which is consistent with the lower accuracy of FASTSIMCOAL2 to estimate more ancient events, such as those involving species formation (Excoffier et al., 2013).

3.5. Inference of past demographic history

STAIRWAY PLOT analyses suggests the three species experienced parallel demographic responses to climate warming since the end of the last glacial period (Figure 5). More specifically, all analysed populations from the three species show demographic declines that generally follow the LGM and reduced their effective population sizes (N_e) by >95 % (Figure 5). We note that these population size estimates differ from those of the parameterized divergence model (Figure 4), but that the divergence model did not include population size change parameters because of the complexity it would have added to the alternative tested models (Knowles, 2009).

3.6. Environmental niche modelling

The low OR_{MTP} ($OR_{MTP} < 0.01$) and high AUC_{TEST} ($AUC_{TEST} > 0.99$) for the ENM of each species indicate their high discriminatory power and low degree of overfitting,

503 respectively (for details on model performance and parameters, see Table S6).
504 Climatically suitable areas predicted by ENMs yield distribution patterns highly
505 congruent with the present-day observed distributions for the three species (Figure 6).
506 Only very small areas in mountain ranges far from the current distribution of each
507 species are (over-) predicted as suitable (Figure 6). Palaeoclimatic reconstructions
508 under both MIROC-ESM and CCSM4 general atmospheric circulation models yield
509 reasonably similar predictions about the distribution of the three species during the
510 LGM (Figure 6), although the extent of the projected distributions varies among the
511 species. The projection of the present-day climate niche envelope to LGM climatic
512 conditions suggests some important changes in the distribution and patterns of
513 population connectivity of the three species (Figure 6). In particular, with a more
514 continuous distribution and overall higher suitability during the LGM than in the
515 present in each species, they are projected to have had considerable overlap in their
516 distributions in the past (Figure 6).
517

518 # 4. DISCUSSION

519 Although genetic evidence of reticulate evolution suggests incomplete reproductive
520 isolation among some Iberian *Podisma* grasshoppers, genetic cohesion has been
521 maintained across each species, even in the face of multiple distribution shifts in
522 response to Pleistocene glacial cycles. However, several lines of evidence suggest that
523 this is not due solely to the rapid evolution of reproductive isolation. Instead, the
524 spatial distribution of sky islands, along with limited dispersal capacity and marked
525 population declines during interglacial periods, may be important factors in
526 maintaining geographic isolation in the face of climate-induced distributional shifts.
527 These insights are only apparent when considering a suite of analyses in which each
528 unveils an aspect of the speciation process, but together convey how divergence
529 across a complex landscape during a dynamic historical period of climate change might
530 have taken place, avoiding a melting pot scenario in which gene flow precludes
531 speciation.
532

533 **4.1. Determinants of species pump or melting pot processes**

In areas with temperate climates, such as the Mediterranean region, cold-adapted species with narrow climatic niches are currently limited to small and isolated patches of high elevation habitat (i.e., sky islands; Flantua et al., 2020; Knowles & Massatti, 2017). Fragmentation of contemporary populations is clearly reflected in patterns of genetic structure within the studied species complex, with all assigned to a unique genetic cluster with a high probability (>0.99) of membership, except for three nearby populations (DEMA, URBI and MON) of *P. carpetana* from the same mountain range (Figure 1). However, during past glacial periods when cooler temperatures predominated, the expansion of temperate climatic conditions into what is now unsuitable habitat are also predicted to drive expansion of cold-adapted species (Hewitt, 2000). Accordingly, range expansions during glacial periods and extreme contractions during interglacials (i.e., current conditions) were inferred in each of the *Podisma* species from environmental niche models (Figure 6). These inferences are corroborated by genomic-based demographic reconstructions that show marked, parallel declines in the population size of each species starting around the onset of the Holocene (Figure 5). Postglacial demographic bottlenecks were dramatic, with effective population sizes reduced to a fraction of those estimated around the LGM. This is consistent with the current distribution of climatically suitable habitats and the low dispersal capability of the species that nowadays persist in small and highly fragmented interglacial refugia (Bennett & Provan, 2008; Stewart et al., 2010). Thus, both extreme isolation and severe demographic bottlenecks after the LGM created the perfect scenario for genetic differentiation via strong genetic drift and a fragmented population structure.

In the different sky island archipelagos of the Iberian Peninsula, like other montane regions across the globe, the repeated climate-induced distributional shifts and associated demographic conditions (e.g., bottlenecked and fragmented populations) experienced by their biotas represent the quintessential setting for a species pump diversification process (Flantua et al., 2020; Haffer, 1969; Papadopoulou & Knowles, 2015a; Wallis et al., 2016). However, this dynamic can transition into a melting pot scenario – that is, the repeated cycles of distributional shifts result in the loss of incipient divergences due to gene flow during range expansions (Klicka & Zink, 1997; Maier et al., 2019). This tipping point between distributional shifts promoting

versus inhibiting speciation is expected to vary among species and geographic settings. The inherent dispersal constraints of flightlessness, coupled with climatic adaptation of *Podisma* grasshoppers to montane and alpine environments, suggests species' traits may indeed contribute to the relative isolation and demographic bottlenecks that promote and maintain genetic differentiation (Papadopoulou & Knowles, 2016; e.g., Ortego et al., 2015; Papadopoulou & Knowles, 2015b; Schoville et al., 2012; Thomaz et al., 2020). With closely related species of insects often distinguished only by male genitalia, it also suggests that sexual selection may play a role in maintaining species boundaries and explain limited hybridization among the studied species during periods of extensive secondary contact (Arnqvist, 1998; Hosken & Stockley, 2004; also see Marquez & Knowles, 2007 for an example in montane grasshoppers in North America). However, biotic factors are not the only determinant of the fate of incipient divergences. The geographic context of climatic-induced distributional shifts of habitats and their constituent inhabitants are also important. That is, the dynamic of colonization itself may be instrumental in determining the distribution of genetic variation and differentiation (see Knowles & Massatti, 2017).

With the sky islands in the Iberian Peninsula embedded in a landscape of unsuitable habitat, the likelihood of dispersal may certainly be reduced, but not impossible, especially with the projections of a more expansive distribution of suitable habitat for temperate taxa in the past (Figure 6). Yet, the presence of past corridors of suitable habitat among the isolated contemporary populations does not necessarily mean that they were utilized or that the three *Podisma* species actually came into secondary contact. Low dispersal ability and a marked philopatric behavior of these flightless species (Barton & Hewitt, 1981, 1982; Mason et al., 1995), ecological constraints (e.g., biotic interactions; Hampe, 2004; Ortego & Knowles, 2020), and the strong fragmentation and small sizes of severely bottlenecked populations (Figures 1 and 5) might have hampered their capacity to colonize remote areas that were climatically suitable during glacial periods (Kearney & Porter, 2009; Wiens et al., 2009). For instance, it is likely the current tiny distribution of *P. cantabricae* (< 25-50 km^2; Presa et al*.,* 2016b) in a topographically highly complex region severely limited its capacity to reach predicted environmentally suitable, but distant areas (i.e., located > 1,000 km away from its current range) during the LGM (Figure 6). In sum, incipient

divergences may be lost among some sky island populations, but not others, and similarly, the opportunity for past hybridization among currently allopatric *Podisma* taxa may depend on the contemporary and past geographic configuration of suitable habitats within the dynamic ranges of each species (Knowles & Massatti, 2017; Tonzo et al., 2021).

When the speciation process is viewed through the lens of divergence with gene flow, rather than divergence in isolation, it invites a shift in perspective about the controls on speciation (Aguilée et al., 2018; Harvey et al., 2019). For example, in addition to the traditional focus on the rate of evolution of reproductive isolation as a control on diversification (in which potential gene flow associated with cycles of climate-induced distributional shifts is thwarted), given that divergence in *Podisma* does not fit a divergence in isolation model (Figures 3 and 4), other factors may be involved in the maintenance of incipient divergence. Both the differences in the relative timing of divergence, as well as differences in inferred gene flow among *Podisma* species and population lineages (Figures 2, 3, and 4), point to varying degrees in the permeability of lineage boundaries. This suggests that the differing consequences of hybridization (i.e., the varied possibilities and effects of gene flow) across the landscape may control diversification dynamics. That is, opportunities and extent of gene flow across the landscape may determine whether repeated distributional shifts act as a species-pump versus a melting pot, not only the rate of reproductive isolation (Aguilée et al., 2018; Dynesius & Jansson, 2014; Harvey et al., 2019).

From this perspective of divergence with gene flow (as opposed to divergence in isolation), in which the rate of reproductive isolation is not the only factor controlling diversification, the timing of divergence can take on new meaning and provide new insights into the speciation process. It is notable that species boundaries are maintained even though some have remained semipermeable for extended periods of time (i.e., introgression between non-sister species *P. pedestris* and *P. carpetana*; Figure 4). In other words, reproductive isolation may be viewed as having been more or less effective in reducing the loss of incipient divergences, especially given that projections of species distributions predict some overlap among all *Podisma*

species during glacial periods. In addition, because these past distributions were not contiguous, but rather some dispersal corridors were more limited in geographic scope than others (Figure 6), it suggests that the opportunities for gene flow (or conversely, the extent of geographic isolation) may have had a prominent effect on the permeability of species boundaries, in addition to any role the rate of reproductive isolation might have played in speciation. In fact, while we cannot exclude the possibility that the rate of evolution of reproductive isolation as a key determinant of the likelihood of speciation (as well as the genetic cohesion of all the species), we can make an argument that Pleistocene speciation in *Podisma* grasshoppers likely had other contributing factors. For example, if speciation was indeed promoted by the fragmentation and isolation of populations during the relatively short interglacial periods, rather than the geologically longer glacial periods when the grasshopper distributions are projected to have been more widespread (Figure 6), it would imply the development of reproductive isolating mechanisms correspondingly much more rapid than in classical models where displacements into isolated glacial refugia promoted speciation (e.g., Hewitt, 1996; Knowles, 2001; also see Klicka & Zink, 1997 and Ebdon et al., 2021 for arguments against Pleistocene speciation because of the rapidity of glacial cycles).

4.2. Determinants of permeable species boundaries

Although ENMs predicted that the distributions of the three taxa largely overlapped during the LGM, genomic data only supported gene flow from *P. pedestris* and *P. carpetana*. Different reasons could explain this specific history of limited introgressive hybridization. Lack of historical hybridization between some species pairs might be a consequence of limited past connectivity and opportunity of gene flow due to geographical isolation (i.e., the geographically distant contemporary ranges of *P. pedestris* and *P. cantabricae*; Figure 1). Alternatively, some of the studied species might have quickly evolved pre- or postzygotic reproductive isolation mechanisms (i.e., speciation in strict isolation) as a by-product of allopatric divergence (Coyne & Orr, 2004) or via reinforcement after secondary contact (Pfennig, 2016; Servedio & Noor, 2003). For instance, the two sister species *P. carpetana* and *P. cantabricae* currently have geographically adjacent distributions in northwestern Iberia (Figure 1), and

multiple instances of secondary contact during the estimated distributional expansions (Figure 6) might have accelerated the rapid evolution of reproductive isolation (Coyne & Orr, 2004; Hoskin et al., 2005). Accordingly, previous studies have found that hybrid dysfunction, genetic incompatibilities and the evolution of pre- and postzygotic reproductive isolation mechanisms is frequent in contact zones between species (Bailey et al., 2004), subspecies (Virdee & Hewitt, 1994), and chromosomal races (Barton & Hewitt, 1981) of montane and alpine grasshoppers.

An intriguing finding is that historical gene flow between *P. pedestris* and *P. carpetana* was asymmetric (Figures 2-4). Unidirectional introgression might have resulted from extensive hybridization during periods of secondary contact followed by repeated backcrossing between hybrids and only one parental species (e.g., Field, Ayre, Whelan, & Young, 2011; Kirschel et al., 2020). Asymmetric gene flow could be also explained by a higher capacity of the donor species to disperse into the range of the recipient one (Jacquemyn et al., 2012; Ortego et al., 2021). In the absence of reproductive barriers, the two species will interbreed and first generation hybrids will more often mate with the most abundant local species, resulting in introgressive hybridization. Although *P. pedestris* is generally a micropterus flightless species, long-winged individuals have been frequently described in the literature (Lemonnier-Darcemont & Darcemont, 2004 and references therein) and this polymorphism has been suggested to favor population connectivity and contribute to the colonization of suitable habitats (Zuna-Kratky et al., 2016). In contrast, the two other *Podisma* species from the Iberian Peninsula are either apterous (*P. cantabricae*) or micropterus (*P. carpetana*) and long-winged forms have never been reported (Morales-Agacino, 1951; Presa et al., 2016a, b). In Orthoptera species presenting wing polymorphism, macropterous forms seem to be occasional and occur at low frequencies within populations. However, these forms have been found to be integral for range expansions at extremely short spatiotemporal scales (Hochkirch & Damerau, 2009), which might be particularly exacerbated under changing environmental conditions such as those imposed by Quaternary climatic oscillations (Simmons & Thomas, 2004). In the context of our study, increased availability of suitable habitats for colonization in the transition from interglacial to glacial periods might have led to selection for macropterous forms in peripheral populations at the expanding margins and favored

693 dispersal of *P. pedestris* within the distribution range of *P. carpetana* (Hochkirch &
694 Damerau, 2009; Noguerales et al., 2016).
695

696 5. CONCLUSIONS

697 Our integrative analyses provided limited evidence of interspecific gene flow during
698 prolonged periods of projected extensive secondary contact and emphasize the
699 genetic cohesiveness of all species within the alpine *Podisma* complex. These findings
700 support the notion that the interplay among Pleistocene-driven isolation (i.e.,
701 confinement in interglacial refugia), landscape composition (i.e., spatial configuration
702 of sky islands), and species´ traits (i.e., flightlessness) can trigger the necessary
703 mechanisms for long-lasting genomic diversification and speciation in alpine and
704 montane biotas (Dynesius & Jansson, 2014; Knowles, 2001). Our comprehensive suite
705 of distributional, demographic and phylogenomic analyses also provided a mechanistic
706 explanation for the uncertain phylogenetic relationships among the studied
707 grasshopper species and collectively highlight the important role of Quaternary
708 climatic oscillations in promoting diversification and genetic fragmentation of relictual
709 alpine organisms from temperate regions that currently persist as highly isolated
710 populations in disparate mountain ranges. Irrespective of which factors control
711 diversification (i.e., the rate of reproductive isolation versus dispersal, and hence
712 opportunities for gene flow), the time of speciation supports a model of Pleistocene
713 divergence. This in its own right, means that *Podisma* grasshoppers of the sky islands
714 from the Iberian Peninsula constitute an ideal system to investigate further some
715 intriguing questions the different independent data types and analytical procedures
716 raise about the speciation process. Future experimental crosses might reveal the
717 presence of pre- and post-zygotic barriers to interspecific gene flow that could clarify
718 whether the absence of genomic evidence for introgressive hybridization among most
719 species-pairs is a consequence of reproductive isolation and the completion of the
720 speciation process or resulted from limited opportunity of hybridization due to
721 population isolation in sky islands and dispersal limitation during range expansions.
722

723 **ACKNOWLEDGEMENTS**

We wish to thank to Amparo Hidalgo-Galiana for library preparation, Victor Noguerales and Pedro J. Cordero for collecting samples from Picos de Europa, Vanina Tonzo and Anna Papadopoulou for help during fieldwork and data analysis, Sergio Pereira (The Centre for Applied Genomics) for Illumina sequencing, and three anonymous referees for their constructive and valuable comments on an earlier version of the manuscript. We thank Spanish and French National Parks and the environmental authorities from each region for providing sampling permissions. We also thank Laboratorio de Ecología Molecular from Estación Biológica de Doñana (LEM-EBD) for logistic support and Centro de Supercomputación de Galicia (CESGA) and Doñana's Singular Scientific-Technical Infrastructure (ICTS-RBD) for access to computer resources. Research was funded by the Spanish Ministry of Economy, Industry and Competitiveness and European Social Fund (grant numbers: CGL2014-54671-P and CGL2017-83433-P).

AUTHOR CONTRIBUTIONS

J.O. and L.L.K. conceived the study and designed the research. J.O. collected the samples and produced and analyzed the data. J.O. led the writing with inputs from L.L.K.

DATA AVAILABILITY STATEMENT

Raw Illumina reads have been deposited at the NCBI Sequence Read Archive (SRA) under BioProject PRJNA759248. Input files for all analyses are available for download on Figshare (https://doi.org/10.6084/m9.figshare.16645912).

CONFLICT OF INTEREST

The authors have no conflicts of interest to declare.

ORCID

Joaquín Ortego https://orcid.org/0000-0003-2709-429X

L. Lacey Knowles https://orcid.org/0000-0002-6567-4853

REFERENCES

Aguilée, R., Gascuel, F., Lambert, A., & Ferriere, R. (2018). Clade diversification dynamics and the biotic and abiotic controls of speciation and extinction rates. *Nature Communications, 9*, 3013. doi:10.1038/s41467-018-05419-7

April, J., Hanner, R. H., Dion-Côté, A. M., & Bernatchez, L. (2013). Glacial cycles as an allopatric speciation pump in north-eastern American freshwater fishes. *Molecular Ecology, 22*(2), 409-422. doi:10.1111/mec.12116

Arnqvist, G. (1998). Comparative evidence for the evolution of genitalia by sexual selection. *Nature, 393*(6687), 784-786. doi:10.1038/31689

Bailey, R. I., Thomas, C. D., & Butlin, R. K. (2004). Premating barriers to gene exchange and their implications for the structure of a mosaic hybrid zone between *Chorthippus brunneus* and *C. jacobsi* (Orthoptera : Acrididae). *Journal of Evolutionary Biology, 17*(1), 108-119. doi:10.1046/j.1420-9101.2003.00648.x

Barton, N. H. (1980). The fitness of hybrids between two chromosomal races of the grasshopper *Podisma pedestris*. *Heredity, 45*(AUG), 47-59. doi:10.1038/hdy.1980.49

Barton, N. H., & Hewitt, G. M. (1981). A chromosomal cline in the grasshopper *Podisma pedestris*. *Evolution, 35*(5), 1008-1018. doi:10.2307/2407871

Barton, N. H., & Hewitt, G. M. (1982). A measurement of dispersal in the grasshopper *Podisma pedestris* (Orthoptera, Acrididae). *Heredity, 48*(APR), 237-249. doi:10.1038/hdy.1982.29

Bennett, K. D., & Provan, J. (2008). What do we mean by refugia? *Quaternary Science Reviews, 27*(27-28), 2449-2455. doi:10.1016/j.quascirev.2008.08.019

Bernardes, J. S., Dávila, A. M., Costa, V. S., & Zaverucha, G. (2007). Improving model construction of profile HMMs for remote homology detection through structural alignment. *BMC Bioinformatics, 8*, 435. doi:10.1186/1471-2105-8-435

Bouckaert, R., Heled, J., Kuhnert, D., Vaughan, T., Wu, C. H., Xie, D., . . . Drummond, A. J. (2014). BEAST2: A software platform for Bayesian evolutionary analysis. *PLoS Computational Biology, 10*(4), e1003537. doi:10.1371/journal.pcbi.1003537

Bouckaert, R. R. (2010). DENSITREE: making sense of sets of phylogenetic trees. *Bioinformatics, 26*(10), 1372-1373. doi:10.1093/bioinformatics/btq110

787 Braconnot, P., Otto-Bliesner, B., Harrison, S., Joussaume, S., Peterchmitt, J. Y., Abe-
788 Ouchi, A., . . . Zhao, Y. (2007). Results of PMIP2 coupled simulations of the Mid-
789 Holocene and Last Glacial Maximum - Part 1: experiments and large-scale
790 features. *Climate of the Past, 3*(2), 261-277. doi:10.5194/cp-3-261-2007
791 Bryant, D., Bouckaert, R., Felsenstein, J., Rosenberg, N. A., & RoyChoudhury, A. (2012).
792 Inferring species trees directly from biallelic genetic markers: Bypassing gene
793 trees in a full coalescent analysis. *Molecular Biology and Evolution, 29*(8), 1917-
794 1932. doi:10.1093/molbev/mss086
795 Burnham, K. P., & Anderson, D. R. (2002). *Model Selection and Multimodel Inference: A*
796 *Practical Information-Theoretic Approach*. New York, NY: Springer.
797 Capella-Gutiérrez, S., Silla-Martínez, J. M., & Gabaldón, T. (2009). TRIMAL: a tool for
798 automated alignment trimming in large-scale phylogenetic analyses.
799 *Bioinformatics, 25*(15), 1972-1973. doi:10.1093/bioinformatics/btp348
800 Carstens, B. C., & Knowles, L. L. (2007). Shifting distributions and speciation: species
801 divergence during rapid climate change. *Molecular Ecology, 16*(3), 619-627.
802 doi:10.1111/j.1365-294X.2006.03167.x
803 Catchen, J., Hohenlohe, P. A., Bassham, S., Amores, A., & Cresko, W. A. (2013). STACKS:
804 an analysis tool set for population genomics. *Molecular Ecology, 22*(11), 3124-
805 3140. doi:10.1111/mec.12354
806 Chifman, J., & Kubatko, L. (2014). Quartet inference from SNP data under the
807 coalescent model. *Bioinformatics, 30*(23), 3317-3324.
808 doi:10.1093/bioinformatics/btu530
809 Cigliano, M. M., Braun, H., Eades, D. C., & Otte, D. (2021). Orthoptera Species File
810 (OSF). Available at http://orthoptera.speciesfile.org (accessed 23 May 2021).
811 Coyne, J. A., & Orr, H.A. (2004). *Speciation*. Sunderland, MA, USA: Sinauer.
812 Danecek, P., Auton, A., Abecasis, G., Albers, C. A., Banks, E., DePristo, M. A., . . . Grp, G.
813 P. A. (2011). The variant call format and VCFTOOLS. *Bioinformatics, 27*(15), 2156-
814 2158. doi:10.1093/bioinformatics/btr330
815 de Manuel, M., Kuhlwilm, M., Frandsen, P., Sousa, V. C., Desai, T., Prado-Martinez, J., . .
816 . Marques-Bonet, T. (2016). Chimpanzee genomic diversity reveals ancient
817 admixture with bonobos. *Science, 354*(6311), 477-481.
818 doi:10.1126/science.aag2602

819 Durand, E. Y., Patterson, N., Reich, D., & Slatkin, M. (2011). Testing for ancient
820 admixture between closely related populations. *Molecular Biology and*
821 *Evolution, 28*(8), 2239-2252. doi:10.1093/molbev/msr048
822 Dynesius, M., & Jansson, R. (2014). Persistence of within-species lineages: A neglected
823 control of speciation rates. *Evolution, 68*(4), 923-934. doi:10.1111/evo.12316
824 Earl, D. A., & vonHoldt, B. M. (2012). STRUCTURE HARVESTER: a website and program for
825 visualizing STRUCTURE output and implementing the Evanno method.
826 *Conservation Genetics Resources, 4*(2), 359-361. doi:10.1007/s12686-011-9548-
827 7
828 Eaton, D. A. R. (2014). PYRAD: assembly of *de novo* RADseq loci for phylogenetic
829 analyses. *Bioinformatics, 30*(13), 1844-1849.
830 doi:10.1093/bioinformatics/btu121
831 Eaton, D. A. R., & Ree, R. H. (2013). Inferring phylogeny and introgression using RADseq
832 data: An example from flowering plants (*Pedicularis*: *Orobanchaceae*).
833 *Systematic Biology, 62*(5), 689-706. doi:10.1093/sysbio/syt032
834 Ebdon, S., Laetsch, D. R., Dapporto, L., Hayward, A., Ritchie, M. G., Dincă, V., Vilá, R. &
835 Lohse, K. (2021) The Pleistocene species pump past its prime: Evidence from
836 European butterfly sister species. *Molecular Ecology*, *30*(14), 3575-3589.
837 doi:10.1111/mec.15981
838 Evanno, G., Regnaut, S., & Goudet, J. (2005). Detecting the number of clusters of
839 individuals using the software STRUCTURE: a simulation study. *Molecular Ecology,*
840 *14*(8), 2611-2620. doi:10.1111/j.1365-294X.2005.02553.x
841 Excoffier, L., Dupanloup, I., Huerta-Sánchez, E., Sousa, V. C., & Foll, M. (2013). Robust
842 demographic inference from genomic and SNP data. *PLoS Genetics, 9*(10),
843 e1003905. doi:10.1371/journal.pgen.1003905
844 Field, D. L., Ayre, D. J., Whelan, R. J., & Young, A. G. (2011). Patterns of hybridization
845 and asymmetrical gene flow in hybrid zones of the rare *Eucalyptus aggregata*
846 and common *E. rubida*. *Heredity, 106*(5), 841-853. doi:10.1038/hdy.2010.127
847 Flantua, S. G. A., Payne, D., Borregaard, M. K., Beierkuhnlein, C., Steinbauer, M. J.,
848 Dullinger, S., . . . Field, R. (2020). Snapshot isolation and isolation history
849 challenge the analogy between mountains and islands used to understand

endemism. *Global Ecology and Biogeography, 29*(10), 1651-1673. doi:10.1111/geb.13155

Gilbert, K. J., Andrew, R. L., Bock, D. G., Franklin, M. T., Kane, N. C., Moore, J. S., . . . Vines, T. H. (2012). Recommendations for utilizing and reporting population genetic analyses: the reproducibility of genetic clustering using the program STRUCTURE. *Molecular Ecology, 21*(20), 4925-4930. doi:10.1111/j.1365-294X.2012.05754.x

González-Serna, M. J., Cordero, P. J., & Ortego, J. (2019). Spatiotemporally explicit demographic modelling supports a joint effect of historical barriers to dispersal and contemporary landscape composition on structuring genomic variation in a red-listed grasshopper. *Molecular Ecology, 28*(9), 2155-2172. doi:10.1111/mec.15086

Haffer, J. (1969). Speciation in Amazonian forest birds. *Science, 165*(3889), 131-137. doi:10.1126/science.165.3889.131

Hampe, A. (2004). Bioclimate envelope models: what they detect and what they hide. *Global Ecology and Biogeography, 13*(5), 469-471. doi:10.1111/j.1466-822X.2004.00090.x

Harvey, M. G., Singhal, S., & Rabosky, D. L. (2019). Beyond reproductive isolation: Demographic controls on the speciation process. In D. J. Futuyma (Ed.), *Annual Review of Ecology, Evolution, and Systematics, Vol 50* (Vol. 50, pp. 75-95). Palo Alto: Annual Reviews.

Hasumi, H., & Emori, S. (2004). *K-1 Coupled GCM (MIROC) Description*. Tokyo, Japan: Center for Climate System Research (CCSR), University of Tokyo; National Institute for Environmental Studies (NIES); Frontier Research Center for Global Change (FRCGC).

Hewitt, G. (2000). The genetic legacy of the Quaternary ice ages. *Nature, 405*(6789), 907-913.

Hewitt, G. M. (1996). Some genetic consequences of ice ages, and their role in divergence and speciation. *Biological Journal of the Linnean Society, 58*(3), 247-276.

Hijmans, R. J., Cameron, S. E., Parra, J. L., Jones, P. G., & Jarvis, A. (2005). Very high resolution interpolated climate surfaces for global land areas. *International Journal of Climatology, 25*(15), 1965-1978. doi:10.1002/joc.1276

Hochkirch, A., & Damerau, M. (2009). Rapid range expansion of a wing-dimorphic bush-cricket after the 2003 climatic anomaly. *Biological Journal of the Linnean Society, 97*(1), 118-127. doi:10.1111/j.1095-8312.2008.01199.x

Hosken, D. J., & Stockley, P. (2004). Sexual selection and genital evolution. *Trends in Ecology & Evolution, 19*(2), 87-93. doi:10.1016/j.tree.2003.11.012

Hoskin, C. J., Higgie, M., McDonald, K. R., & Moritz, C. (2005). Reinforcement drives rapid allopatric speciation. *Nature, 437*(7063), 1353-1356. doi:10.1038/nature04004

Huang, H. T., & Knowles, L. L. (2016). Unforeseen consequences of excluding missing data from next-generation sequences: Simulation study of RAD sequences. *Systematic Biology, 65*(3), 357-365. doi:10.1093/sysbio/syu046

Jacquemyn, H., Brys, R., Honnay, O., & Roldán-Ruiz, I. (2012). Asymmetric gene introgression in two closely related *Orchis* species: evidence from morphometric and genetic analyses. *BMC Evolutionary Biology, 12*, 178. doi:10.1186/1471-2148-12-178

Jakobsson, M., & Rosenberg, N. A. (2007). CLUMPP: a cluster matching and permutation program for dealing with label switching and multimodality in analysis of population structure. *Bioinformatics, 23*(14), 1801-1806. doi:10.1093/bioinformatics/btm233

Janes, J. K., Miller, J. M., Dupuis, J. R., Malenfant, R. M., Gorrell, J. C., Cullingham, C. I., & Andrew, R. L. (2017). The *K*=2 conundrum. *Molecular Ecology, 26*(14), 3594-3602. doi:10.1111/mec.14187

Jombart, T. (2008). *Adegenet*: a R package for the multivariate analysis of genetic markers. *Bioinformatics, 24*(11), 1403-1405. doi:10.1093/bioinformatics/btn129

Kearney, M., & Porter, W. (2009). Mechanistic niche modelling: combining physiological and spatial data to predict species' ranges. *Ecology Letters, 12*(4), 334-350. doi:10.1111/j.1461-0248.2008.01277.x

911 Keightley, P. D., Ness, R. W., Halligan, D. L., & Haddrill, P. R. (2014). Estimation of the
912 spontaneous mutation rate per nucleotide site in a *Drosophila melanogaster*
913 full-sib family. *Genetics, 196*(1), 313-320. doi:10.1534/genetics.113.158758
914 Keightley, P. D., Pinharanda, A., Ness, R. W., Simpson, F., Dasmahapatra, K. K., Mallet,
915 J., . . . Jiggins, C. D. (2015). Estimation of the spontaneous mutation rate in
916 *Heliconius melpomene*. *Molecular Biology and Evolution, 32*(1), 239-243.
917 doi:10.1093/molbev/msu302
918 Keller, I., Veltsos, P., & Nichols, R. A. (2008). The frequency of rDNA variants within
919 individuals provides evidence of population history and gene flow across a
920 grasshopper hybrid zone. *Evolution, 62*(4), 833-844. doi:10.1111/j.1558-
921 5646.2008.00320.x
922 Kirschel, A. N. G., Nwankwo, E. C., Pierce, D. K., Lukhele, S. M., Moysi, M., Ogolowa, B.
923 O., . . . Brelsford, A. (2020). CYP2J19 mediates carotenoid colour introgression
924 across a natural avian hybrid zone. *Molecular Ecology, 29*(24), 4970-4984.
925 doi:10.1111/mec.15691
926 Klicka, J., & Zink, R. M. (1997). The importance of recent ice ages in speciation: A failed
927 paradigm. *Science, 277*(5332), 1666-1669. doi:10.1126/science.277.5332.1666
928 Knowles, L. L. (2001). Genealogical portraits of speciation in montane grasshoppers
929 (genus *Melanoplus*) from the sky islands of the Rocky Mountains. *Proceedings*
930 *of the Royal Society B-Biological Sciences, 268*(1464), 319-324.
931 doi:10.1098/rspb.2000.1364
932 Knowles, L. L. (2009). Statistical phylogeography. *Annual Review of Ecology Evolution*
933 *and Systematics, 40*, 593-612. doi:10.1146/annurev.ecolsys.38.091206.095702
934 Knowles, L. L., & Carstens, B. C. (2007). Estimating a geographically explicit model of
935 population divergence. *Evolution, 61*(3), 477-493. doi:10.1111/j.1558-
936 5646.2007.00043.x
937 Knowles, L. L., & Massatti, R. (2017). Distributional shifts - not geographic isolation - as
938 a probable driver of montane species divergence. *Ecography, 40*(12), 1475-
939 1485. doi:10.1111/ecog.02893
940 Kutschera, V. E., Bidon, T., Hailer, F., Rodi, J. L., Fain, S. R., & Janke, A. (2014). Bears in a
941 forest of gene trees: Phylogenetic inference is complicated by incomplete

lineage sorting and gene flow. *Molecular Biology and Evolution, 31*(8), 2004-2017. doi:10.1093/molbev/msu186

Lemonnier-Darcemont, M., & Darcemont, C. (2014). New observation of *Podisma pedestris* (Linne, 1758) forma macroptera (Orthoptera, Acrididae), in the Republic of Macedonia. *Articulata, 29*(1-2), 1-7.

Liu, C. R., Berry, P. M., Dawson, T. P., & Pearson, R. G. (2005). Selecting thresholds of occurrence in the prediction of species distributions. *Ecography, 28*(3), 385-393. doi:10.1111/j.0906-7590.2005.03957.x

Liu, X. M., & Fu, Y. X. (2015). Exploring population size changes using SNP frequency spectra. *Nature Genetics, 47*(5), 555-559. doi:10.1038/ng.3254

Liu, X. M., & Fu, Y. X. (2020). Stairway Plot 2: demographic history inference with folded SNP frequency spectra. *Genome Biology, 21*(1). doi:10.1186/s13059-020-02196-9

Maddison, W. P., & Knowles, L. L. (2006). Inferring phylogeny despite incomplete lineage sorting. *Systematic Biology, 55*(1), 21-30. doi:10.1080/10635150500354928

Maier, P. A., Vandergast, A. G., Ostoja, S. M., Aguilar, A., & Bohonak, A. J. (2019). Pleistocene glacial cycles drove lineage diversification and fusion in the Yosemite toad (*Anaxyrus canorus*). *Evolution, 73*(12), 2476–2496. doi:10.1111/evo.13868

Mallet, J., Besansky, N., & Hahn, M. W. (2016). How reticulated are species? *Bioessays, 38*(2), 140-149. doi:10.1002/bies.201500149

Manichaikul, A., Mychaleckyj, J. C., Rich, S. S., Daly, K., Sale, M., & Chen, W. M. (2010). Robust relationship inference in genome-wide association studies. *Bioinformatics, 26*(22), 2867-2873. doi:10.1093/bioinformatics/btq559

Marquez, E. J., & Knowles, L. L. (2007). Correlated evolution of multivariate traits: detecting co-divergence across multiple dimensions. *Journal of Evolutionary Biology, 20*(6), 2334-2348. doi:10.1111/j.1420-9101.2007.01415.x

Mason, P. L., Nichols, R. A., & Hewitt, G. M. (1995). Philopatry in the alpine grasshopper *Podisma pedestris* - A novel experimental and analytical method. *Ecological Entomology, 20*(2), 137-145. doi:10.1111/j.1365-2311.1995.tb00439.x

McBreen, K., & Lockhart, P. J. (2006). Reconstructing reticulate evolutionary histories of plants. *Trends in Plant Science, 11*(8), 398-404. doi:10.1016/j.tplants.2006.06.004

Melo-Ferreira, J., Boursot, P., Suchentrunk, F., Ferrand, N., & Alves, P. C. (2005). Invasion from the cold past: extensive introgression of mountain hare (*Lepus timidus*) mitochondrial DNA into three other hare species in northern Iberia. *Molecular Ecology, 14*(8), 2459-2464. doi:10.1111/j.1365-294X.2005.02599.x

Morales-Agacino, E. (1951). Breves notas sobre los *Podismini* de la península ibérica (Orth. Acrid.). *EOS, Tomo extraordinario*, 367-384.

Muscarella, R., Galante, P. J., Soley-Guardia, M., Boria, R. A., Kass, J. M., Uriarte, M., & Anderson, R. P. (2014). *ENMeval*: An R package for conducting spatially independent evaluations and estimating optimal model complexity for MAXENT ecological niche models. *Methods in Ecology and Evolution, 5*(11), 1198-1205. doi:10.1111/2041-210x.12261

Nevado, B., Contreras-Ortiz, N., Hughes, C., & Filatov, D. A. (2018). Pleistocene glacial cycles drive isolation, gene flow and speciation in the high-elevation Andes. *New Phytologist, 219*(2), 779-793. doi:10.1111/nph.15243

Noguerales, V., Cordero, P. J., & Ortego, J. (2018). Integrating genomic and phenotypic data to evaluate alternative phylogenetic and species delimitation hypotheses in a recent evolutionary radiation of grasshoppers. *Molecular Ecology, 27*(5), 1229-1244. doi:10.1111/mec.14504

Noguerales, V., García-Navas, V., Cordero, P. J., & Ortego, J. (2016). The role of environment and core-margin effects on range-wide phenotypic variation in a montane grasshopper. *Journal of Evolutionary Biology, 29*(11), 2129-2142. doi:10.1111/jeb.12915

Nylander, J. A. A., Olsson, U., Alstrom, P., & Sanmartín, I. (2008). Accounting for phylogenetic uncertainty in biogeography: A Bayesian approach to dispersal-vicariance analysis of the thrushes (Aves: *Turdus*). *Systematic Biology, 57*(2), 257-268. doi:10.1080/10635150802044003

Ortego, J., García-Navas, V., Noguerales, V., & Cordero, P. J. (2015). Discordant patterns of genetic and phenotypic differentiation in five grasshopper species

codistributed across a microreserve network. *Molecular Ecology, 24*(23), 5796-5812. doi:10.1111/mec.13426

Ortego, J., Gugger, P. F., & Sork, V. L. (2018). Genomic data reveal cryptic lineage diversification and introgression in Californian golden cup oaks (section *Protobalanus*). *New Phytologist, 218*(2), 804-818. doi:10.1111/nph.14951

Ortego, J., Gutiérrez-Rodríguez, J., & Noguerales, V. (2021) Demographic consequences of dispersal-related trait shift in two recently diverged taxa of montane grasshoppers. *Evolution*, *75*(8), 1998-2013. doi:10.1111/evo.14205

Ortego, J., & Knowles, L. L. (2020). Incorporating interspecific interactions into phylogeographic models: A case study with Californian oaks. *Molecular Ecology, 29*(23), 4510-4524. doi:10.1111/mec.15548

Papadopoulou, A., & Knowles, L. L. (2015a). Genomic tests of the species-pump hypothesis: Recent island connectivity cycles drive population divergence but not speciation in Caribbean crickets across the Virgin Islands. *Evolution, 69*(6), 1501-1517. doi:10.1111/evo.12667

Papadopoulou, A., & Knowles, L. L. (2015b). Species-specific responses to island connectivity cycles: refined models for testing phylogeographic concordance across a Mediterranean Pleistocene Aggregate Island Complex. *Molecular Ecology, 24*(16), 4252-4268. doi:10.1111/mec.13305

Papadopoulou, A., & Knowles, L. L. (2016). Toward a paradigm shift in comparative phylogeography driven by trait-based hypotheses. *Proceedings of the National Academy of Sciences of the United States of America, 113*(29), 8018-8024. doi:10.1073/pnas.1601069113

Papes, M., & Gaubert, P. (2007). Modelling ecological niches from low numbers of occurrences: assessment of the conservation status of poorly known viverrids (Mammalia, Carnivora) across two continents. *Diversity and Distributions, 13*(6), 890-902. doi:10.1111/j.1472-4642.2007.00392.x

Payseur, B. A., & Rieseberg, L. H. (2016). A genomic perspective on hybridization and speciation. *Molecular Ecology, 25*(11), 2337-2360. doi:10.1111/mec.13557

Peterson, B. K., Weber, J. N., Kay, E. H., Fisher, H. S., & Hoekstra, H. E. (2012). Double digest RADseq: An inexpensive method for *de novo* SNP discovery and

genotyping in model and non-model species. *PLoS One, 7*(5), e37135. doi:10.1371/journal.pone.0037135

Petit, R. J., Aguinagalde, I., de Beaulieu, J. L., Bittkau, C., Brewer, S., Cheddadi, R., . . . Vendramin, G. G. (2003). Glacial refugia: Hotspots but not melting pots of genetic diversity. *Science, 300*(5625), 1563-1565.

Pfennig, K. S. (2016). Reinforcement as an initiator of population divergence and speciation. *Current Zoology, 62*(2), 145-154. doi:10.1093/cz/zow033

Phillips, S. J., Anderson, R. P., & Schapire, R. E. (2006). Maximum entropy modeling of species geographic distributions. *Ecological Modelling, 190*(3-4), 231-259. doi:10.1016/j.ecolmodel.2005.03.026

Phillips, S. J., & Dudik, M. (2008). Modeling of species distributions with MAXENT: new extensions and a comprehensive evaluation. *Ecography, 31*(2), 161-175. doi:10.1111/j.0906-7590.2008.5203.x

Pickrell, J. K., & Pritchard, J. K. (2012). Inference of population splits and mixtures from genome-wide allele frequency data. *PLoS Genetics, 8*(11), e1002967. doi:10.1371/journal.pgen.1002967

Presa, J. J., García, M., Clemente, M., Barranco Vega, P., Correas, J., Ferreira, S., Hochkirch, A., Lemos, P., Odé, B., & Prunier, F. (2016a). *Podisma carpetana: The IUCN Red List of Threatened Species 2016* (Publication no. e.T16084405A75089074). https://doi.org/10.2305/IUCN.UK.2016-3.RLTS.T16084405A75089074.en. Retrieved from https://www.iucnredlist.org/species/16084405/75089074 (accessed 23 May 2021).

Presa, J. J., García, M., Clemente, M., Barranco Vega, P., Correas, J., Ferreira, S., Hochkirch, A., Lemos, P., Odé, B. & Prunier, F. (2016b). *Podisma cantabricae: The IUCN Red List of Threatened Species 2016* (Publication no. e.T16084528A75089065. https://doi.org/10.2305/IUCN.UK.2016-3.RLTS.T16084528A75089065.en. Retrieved from https://www.iucnredlist.org/species/16084528/75089065 (accessed 23 May 2021).

Pritchard, J. K., Stephens, M., & Donnelly, P. (2000). Inference of population structure using multilocus genotype data. *Genetics, 155*(2), 945-959.

R Core Team. (2021). R*: A language and environment for statistical computing*. Vienna, Austria: R Foundation for Statistical Computing. Available at https://www.R-project.org/ (accessed May 23, 2021).

Rangel, T. F., Colwell, R. K., Graves, G. R., Fucikova, K., Rahbek, C., & Diniz, J. A. F. (2015). Phylogenetic uncertainty revisited: Implications for ecological analyses. *Evolution, 69*(5), 1301-1312. doi:10.1111/evo.12644

Rosenberg, N. A. (2004). DISTRUCT: a program for the graphical display of population structure. *Molecular Ecology Notes, 4*(1), 137-138. doi:10.1046/j.1471-8286.2003.00566.x

Rosindell, J., Cornell, S. J., Hubbell, S. P., & Etienne, R. S. (2010). Protracted speciation revitalizes the neutral theory of biodiversity. *Ecology Letters, 13*(6), 716-727. doi:10.1111/j.1461-0248.2010.01463.x

Schoville, S. D., Roderick, G. K., & Kavanaugh, D. H. (2012). Testing the 'Pleistocene species pump' in alpine habitats: lineage diversification of flightless ground beetles (Coleoptera: Carabidae: Nebria) in relation to altitudinal zonation. *Biological Journal of the Linnean Society, 107*(1), 95-111. doi:10.1111/j.1095-8312.2012.01911.x

Schrago, C. G., & Seuanez, H. N. (2019). Large ancestral effective population size explains the difficult phylogenetic placement of owl monkeys. *American Journal of Primatology, 81*(3), e22955. doi:10.1002/ajp.22955

Servedio, M. R., & Noor, M. A. F. (2003). The role of reinforcement in speciation: Theory and data. *Annual Review of Ecology Evolution and Systematics, 34*, 339-364. doi:10.1146/annurev.ecolsys.34.011802.132412

Shcheglovitova, M., & Anderson, R. P. (2013). Estimating optimal complexity for ecological niche models: A jackknife approach for species with small sample sizes. *Ecological Modelling, 269*, 9-17. doi:10.1016/j.ecolmodel.2013.08.011

Simmons, A. D., & Thomas, C. D. (2004). Changes in dispersal during species' range expansions. *American Naturalist, 164*(3), 378-395. doi:10.1086/423430

Solís-Lemus, C., Bastide, P., & Ane, C. (2017). PHYLONETWORKS: A package for phylogenetic networks. *Molecular Biology and Evolution, 34*(12), 3292-3298. doi:10.1093/molbev/msx235

1099 Stamatakis, A. (2014). RAXML version 8: a tool for phylogenetic analysis and post-
1100 analysis of large phylogenies. *Bioinformatics, 30*(9), 1312-1313.
1101 doi:10.1093/bioinformatics/btu033
1102 Stewart, J. R., Lister, A. M., Barnes, I., & Dalen, L. (2010). Refugia revisited:
1103 individualistic responses of species in space and time. *Proceedings of the Royal*
1104 *Society B-Biological Sciences, 277*(1682), 661-671. doi:10.1098/rspb.2009.1272
1105 Sukumaran, J., & Knowles, L. L. (2017). Multispecies coalescent delimits structure, not
1106 species. *Proceedings of the National Academy of Sciences of the United States*
1107 *of America, 114*(7), 1607-1612. doi:10.1073/pnas.1607921114
1108 Swofford, D. L. (2002). *PAUP*. Phylogenetic analysis using parsimony (*and other*
1109 *methods). Version 4*. Sunderland, MA: Sinauer Associates.
1110 Takahashi, T., Nagata, N., & Sota, T. (2014). Application of RAD-based phylogenetics to
1111 complex relationships among variously related taxa in a species flock.
1112 *Molecular Phylogenetics and Evolution, 80*, 137-144.
1113 doi:10.1016/j.ympev.2014.07.016
1114 Tariel, J., Longo, G. C., & Bernardi, G. (2016). Tempo and mode of speciation in
1115 *Holacanthus* angelfishes based on RADseq markers. *Molecular Phylogenetics*
1116 *and Evolution, 98*, 84-88. doi:10.1016/j.ympev.2016.01.010
1117 Thom, G., Do Amaral, F. R., Hickerson, M. J., Aleixo, A., Araujo-Silva, L. E., Ribas, C. C., . .
1118 . Miyaki, C. Y. (2018). Phenotypic and genetic structure support gene flow
1119 generating gene tree discordances in an Amazonian floodplain endemic
1120 species. *Systematic Biology, 67*(4), 700-718. doi:10.1093/sysbio/syy004
1121 Thomaz, A. T., & Knowles, L. L. (2020). Common barriers, but temporal dissonance:
1122 Genomic tests suggest ecological and paleo-landscape sieves structure a
1123 coastal riverine fish community. *Molecular Ecology, 29*(4), 783-796.
1124 doi:10.1111/mec.15357
1125 Thome, M. T. C., & Carstens, B. C. (2016). Phylogeographic model selection leads to
1126 insight into the evolutionary history of four-eyed frogs. *Proceedings of the*
1127 *National Academy of Sciences of the United States of America, 113*(29), 8010-
1128 8017. doi:10.1073/pnas.1601064113
1129 Tonzo, V., & Ortego, J. (2021). Glacial connectivity and current population
1130 fragmentation in sky islands explain the contemporary distribution of genomic

variation in two narrow-endemic montane grasshoppers from a biodiversity hotspot. *Diversity and Distributions*, *27*(9), 1619-1633. doi:10.1111/ddi.13306

van Proosdij, A. S. J., Sosef, M. S. M., Wieringa, J. J., & Raes, N. (2016). Minimum required number of specimen records to develop accurate species distribution models. *Ecography, 39*(6), 542-552. doi:10.1111/ecog.01509

Virdee, S. R., & Hewitt, G. M. (1994). Clines for hybrid dysfunction in a grasshopper hybrid zone. *Evolution, 48*(2), 392-407. doi:10.2307/2410100

Wachter, G. A., Papadopoulou, A., Muster, C., Arthofer, W., Knowles, L. L., Steiner, F. M., & Schlick-Steiner, B. C. (2016). Glacial refugia, recolonization patterns and diversification forces in Alpine-endemic *Megabunus* harvestmen. *Molecular Ecology, 25*(12), 2904-2919. doi:10.1111/mec.13634

Wallis, G. P., Waters, J. M., Upton, P., & Craw, D. (2016). Transverse alpine speciation driven by glaciation. *Trends in Ecology & Evolution, 31*(12), 916-926. doi:10.1016/j.tree.2016.08.009

Wen, D. Q., Yu, Y., Hahn, M. W., & Nakhleh, L. (2016). Reticulate evolutionary history and extensive introgression in mosquito species revealed by phylogenetic network analysis. *Molecular Ecology, 25*(11), 2361-2372. doi:10.1111/mec.13544

Wiens, J. A., Stralberg, D., Jongsomjit, D., Howell, C. A., & Snyder, M. A. (2009). Niches, models, and climate change: Assessing the assumptions and uncertainties. *Proceedings of the National Academy of Sciences of the United States of America, 106*, 19729-19736. doi:10.1073/pnas.0901639106

Wisz, M. S., Hijmans, R. J., Li, J., Peterson, A. T., Graham, C. H., Guisan, A., & Distribut, N. P. S. (2008). Effects of sample size on the performance of species distribution models. *Diversity and Distributions, 14*(5), 763-773. doi:10.1111/j.1472-4642.2008.00482.x

Zuna-Kratky, T., Fontana, P., Roesti, C., Braud, Y., Hochkirch, A., Monnerat, C., Rutschmann, F., & Presa, J. J. (2016). *Podisma pedestris: The IUCN Red List of Threatened Species 2016* (Publication no. e.T16084622A70645980). Retrieved from https://www.iucnredlist.org/species/16084622/70645980 (accessed 23 May 2021).

SUPPORTING INFORMATION

Additional supporting information may be found online in the Supporting Information section.

Legends of Supplementary Tables and Figures

TABLE S1 Geographical location and number of analyzed individuals (*n*) for the studied populations of *Podisma pedestris*, *P. carpetana* and *P. cantabricae*. *Cophopodisma pyrenaea* was used as an outgroup in phylogenomic analyses.

TABLE S2 Distribution of topologies (%) contained in 95% highest posterior density (HPD) tree sets reconstructed with SNAPP. Population codes are described in Table S1.

TABLE S3 Analyses of introgression using four-taxon *D*-statistic (ABBA/BABA) tests. Analyses were performed for each of the six species-population combinations separately and using six genomic datasets generated in PYRAD by setting different clustering thresholds (W_{clust} = 0.85 and 0.90) and values for minimum taxon coverage (*minCov* = 10, 20 and 30). *Cophopodisma pyrenaea* was used as an outgroup. All tests were highly significant ($q < 0.001$) after a false discovery rate (FDR) adjustment (5%) to control for multiple tests. Population codes are described in Table S1.

TABLE S4 Comparison of alternative species divergence models (detailed in Figure S1) tested using FASTSIMCOAL2, with best supported models highlighted in bold. Analyses were performed for each of the six species-population combinations separately. Population codes are described in Table S1. The number of loci retained for the calculation of the SFS is indicated in parentheses.

TABLE S5 Demographic parameters inferred with FASTSIMCOAL2 for the most likely species divergence model (Model B, illustrated in Figure S1). Table shows point estimates and lower and upper 95% confidence intervals for each parameter: the ancestral (θ_{ANC}, $\theta_{CAN\text{-}CAR}$) and contemporary (θ_{PED}, θ_{CAR}, θ_{CAN}) effective population sizes, migration rates (*m*), timing of species split (T_{DIV1}, T_{DIV2}), and timing (beginning and end) of interspecific gene flow ($T_{INTROG1}$, $T_{INTROG2}$), with time given in units of generations (or

years, with 1 generation per year). Analyses were performed for each of the six species-population combinations separately. Population codes are described in Table S1.

TABLE S6 Environmental niche modeling (ENM) for *Podisma pedestris*, *P. carpetana* and *P. cantabricae*. Table shows the parameters of the best species-specific model and the variables retained sorted from higher to lower values of permutation importance. Variables in bold are those that cumulatively contributed > 50% to the model based on the permutation importance statistic.

FIGURE S1 Alternative species divergence models tested using FASTSIMCOAL2. Parameters include ancestral (θ_{ANC}, $\theta_{CAN\text{-}CAR}$) and contemporary (θ_{PED}, θ_{CAR}, θ_{CAN}) effective population sizes, migration rates (*m*, arrows), timing of species split (T_{DIV1}, T_{DIV2}), and timing (beginning and end) of interspecific gene flow ($T_{INTROG1}$, $T_{INTROG2}$).

FIGURE S2 Number of reads per individual before and after different quality filtering steps by PYRAD. The cumulative stacked bars represent the total number of raw reads for each individual. Dark red color represents the reads that were discarded by *process_radtags* in STACKS due to low quality, adapter contamination or ambiguous barcode. Light red color represents the reads that were discarded during *step 2* in PYRAD after filtering out reads that did not comply with the quality criteria (reads with >2 sites with a Phred quality score < 20 were discarded). Green color represents the total number of retained reads used to identify homologous loci. Individuals are sorted by species and populations following the same order and codes presented in Table S1.

FIGURE S3 Mean (±SD) log probability of the data (LnPr(X|*K*)) over 10 runs of STRUCTURE (left axes, black dots and error bars) for each value of *K* and the magnitude of Δ*K* (right axes, blue dots). Hierarchical STRUCTURE analyses were run for (a) all species and independently for populations of (b) *Podisma pedestris* and (c) *P. carpetana*. Analyses are based on a random subset of 10,000 SNPs.

FIGURE S4 Principal component analyses (PCAs) of genetic variation for *Podisma pedestris*, *P. carpetana*, and *P. cantabricae*. Analyses were run for all (a) species

(23,333 SNPs) and independently for populations of (b) *P. carpetana* (13,003 SNPs) and (c) *P. pedestris* (11,999 SNPs). Population codes are described in Table S1.

FIGURE S5 Phylogenetic trees inferred with SVDQUARTETS using six genomic datasets generated in PYRAD by setting different clustering thresholds (W_{clust} = 0.85 and 0.90) and values for minimum taxon coverage (*minCov* = 10, 20 and 30). *Cophopodisma pyrenaea* was used as an outgroup. Node colors indicate bootstrapping support (BS) values based on 100 replicates (green: BS > 95 %; orange: 95 % > BS > 90 %; red: BS < 90 %). The number of SNPs retained for each analysis is presented in parentheses. Population codes are described in Table S1.

FIGURE S6 Summary of model fit with PHYLONETWORKS. The figure shows the negative log pseudo-likelihood for models with different number of introgression events (*h* from 0 to 5).

FIGURE S7 Summary of model fit with TREEMIX. The figure shows the Ln(likelihood) for models with different number of migration events (*m* from 0 to 4) over three independent runs (open circles). Analyses were run including one terminal per species and considering six species-population combinations. Codes of the specific populations of each species included in the different analyses are indicated in each panel and described in Table S1.

FIGURE S8 Maximum-likelihood trees inferred with TREEMIX showing the most likely migration event (*m* = 1). The direction of gene flow is represented with an arrow colored according to the percentage of alleles (weight) originating from the source. Analyses were run including one terminal per species and considering six species-population combinations. The number of SNPs retained for each analysis is presented in parentheses. Codes of the specific populations of each species included in the different analyses are described in Table S1.

TABLE 1 Analyses of introgression using four-taxon *D*-statistic (ABBA/BABA) tests. Analyses were performed for each of the six species-population combinations separately using *Cophopodisma pyrenaea* as an outgroup. All tests were highly significant ($q < 0.001$) after a false discovery rate (FDR) adjustment (5%) to control for multiple tests. Population codes are described in Table S1.

P1 (*P. cantabricae)*	P2 (*P. carpetana*)	P3 (*P. pedestris)*	*n*	BABA	ABBA	*D* (± S.D.)	*z*	*q*
DIA	EUR	AUL	3,772	595	932	0.221 ± 0.031	7.08	<0.001
DIA	MON	AUL	3,601	546	990	0.289 ± 0.031	9.29	<0.001
DIA	GUA	AUL	3,553	577	948	0.244 ± 0.033	7.45	<0.001
DIA	EUR	AIG	3,808	592	961	0.238 ± 0.031	7.70	<0.001
DIA	MON	AIG	3,640	551	1,026	0.301 ± 0.031	9.86	<0.001
DIA	GUA	AIG	3,587	566	962	0.259 ± 0.031	8.46	<0.001

n, number of retained SNPs; *D* (± S.D.), *D*-statistic and corresponding standard deviation; *z*, *z*-statistic; *q*, *p*-values adjusted at a FDR of 5%

FIGURE 1 (a) Results of genetic assignments for *Podisma pedestris*, *P. carpetana*, and *P. cantabricae* based on the Bayesian method implemented in the program STRUCTURE. Hierarchical STRUCTURE analyses were run for all species and independently for populations of *P. pedestris* and *P. carpetana*. Analyses are based on a random subset of 10,000 SNPs. Thin vertical lines separate individuals and thick lines demarcate sampling sites, with each individual partitioned into *K* colored segments proportional to the individual's estimated ancestry proportions; population codes are described in Table S1. (b) Map shows sampling localities (black dots with white rings) across the northern half of the Iberian Peninsula (see map inset for focal area), main geographical features (mountain ranges), and the distribution of each taxon (red: *P. pedestris*; blue: *P. carpetana*; green: *P. cantabricae*) as predicted by species-specific environmental niche models (ENM). A white star indicates the sampling locality for the outgroup *Cophopodisma pyrenaea*. Elevation shown by grey shading, with darker areas corresponding to higher elevations.

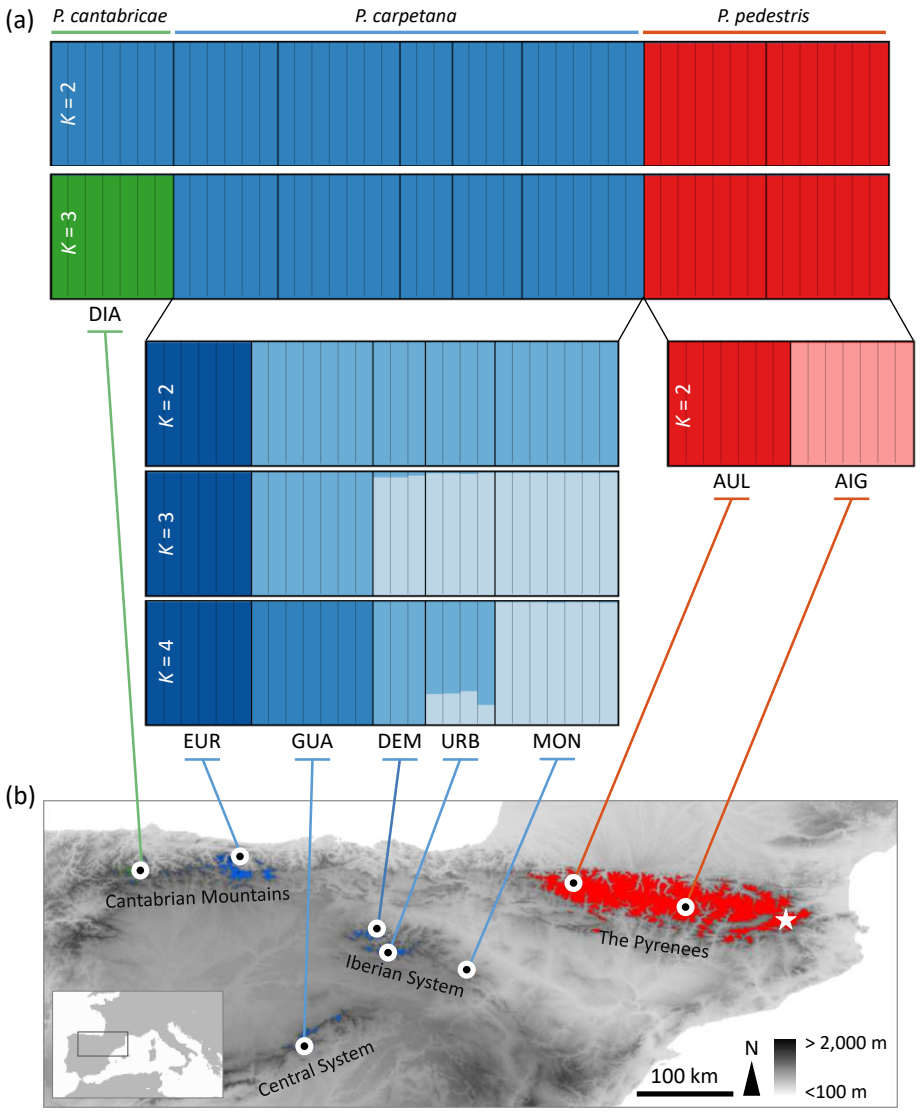

1283

FIGURE 2 Phylogenetic estimates from (a) SNAPP (2,287 SNPs), (b) SVDQUARTETS (20,937 SNPs), and (c) PHYLONETWORKS (1,447 loci) with the different species demarcated by different shaded colors. Bayesian posterior probabilities (for SNAPP) and bootstrapping support values (for SVDQUARTETS) are indicated on the nodes (* = 1), and the inferred inheritance probabilities (γ_A and γ_B) for each parent are shown on the PHYLONETWORKS tree. Population codes are described in Table S1. Picture shows a male of *P. pedestris*, which is morphologically similar to the other two species.

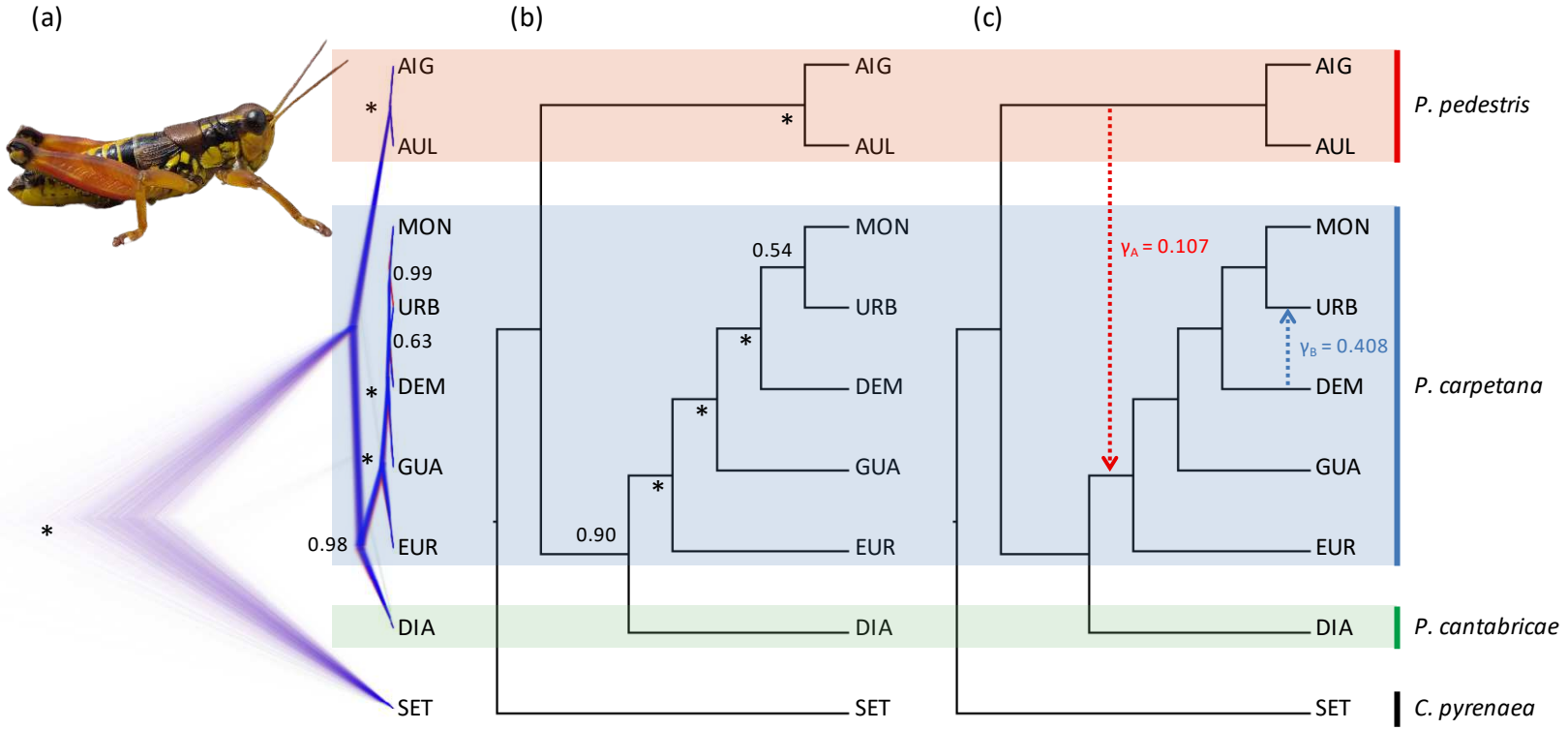

1290

FIGURE 3 Maximum-likelihood tree inferred with TREEMIX (4,569 SNPs) showing the most likely migration event (*m* = 1). The direction of gene flow is represented with an arrow colored according to the percentage of alleles (weight) originating from the source. Codes of the specific populations of each species included in the analysis are described in Table S1. Note that analogous TREEMIX analyses were run considering all other species-population combinations (see Figure S8).

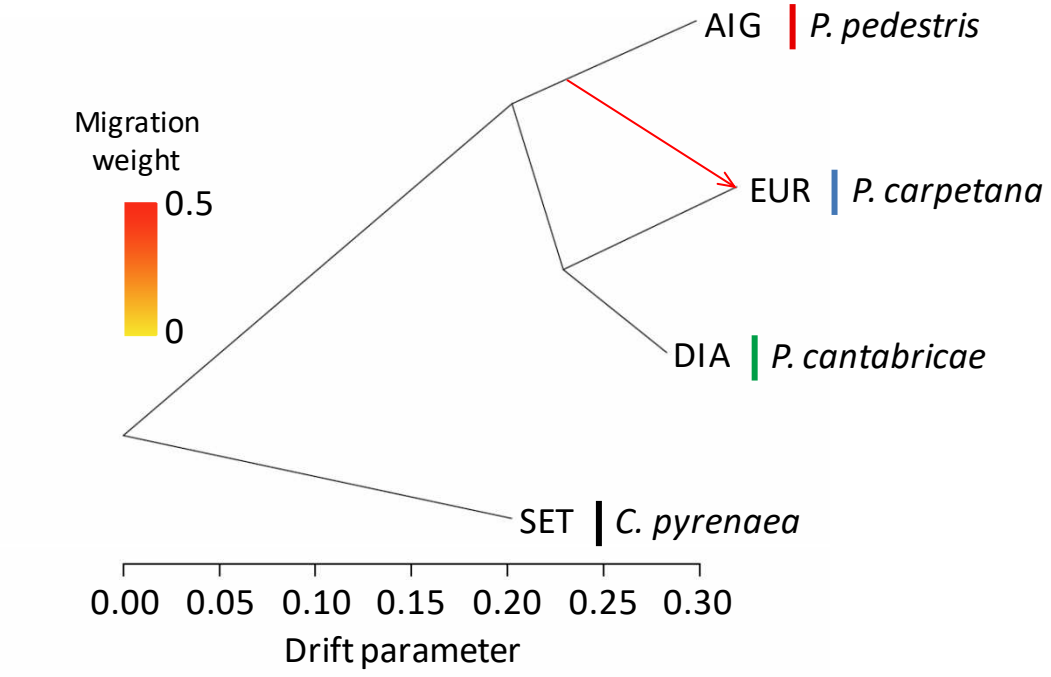

FIGURE 4 Demographic parameters inferred with FASTSIMCOAL2 for the most likely species divergence model (Model B, a divergence with gene flow model; see Tables S4 and S5). Table shows point estimates and lower and upper 95% confidence intervals (in brackets) for each parameter: the ancestral (θ_{ANC}, $\theta_{CAN\text{-}CAR}$) and contemporary (θ_{PED}, θ_{CAR}, θ_{CAN}) effective population sizes, migration rates (*m*), timing of species split (T_{DIV1}, T_{DIV2}), and timing (beginning and end) of interspecific gene flow ($T_{INTROG1}$, $T_{INTROG2}$), with time given in units of generations (or years, with 1 generation per year). Codes of the specific populations (AUL, EUR, and DIA) of each species included in the analysis are described in Table S1. Parameter estimates for analogous FASTSIMCOAL2 analyses run considering all other species-population combinations are presented in Table S5. *Note the effective population size of *Podisma cantabricae* (θ_{CAN}) was calculated from

the level of nucleotide diversity (π) and fixed in FASTSIMCOAL2 analyses (see the Materials and Methods section for further details).

(a)

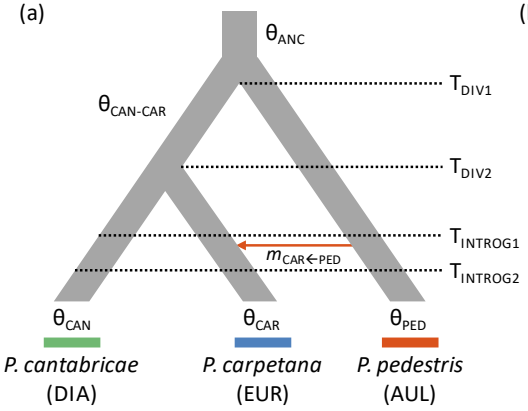

(b)

Parameter	Point estimate	95% CIs
θ_{ANC}	155,653	[29,151 – 418,990]
$\theta_{CAN-CAR}$	127,882	[47,710 – 194,084]
θ_{PED}	46,363	[39,453 – 55,707]
θ_{CAR}	64,394	[60,041 – 79,249]
θ_{CAN}*	71,429	-
T_{DIV1}	992,317	[178,271 – 1,086,881]
T_{DIV2}	135,537	[132,699 – 169,645]
$T_{INTROG1}$	108,047	[106,212 – 158,920]
$T_{INTROG2}$	104,545	[74,192 – 132,094]
$m_{CAR←PED}$	7.75×10^{-04}	$[1.00 \times 10^{-05} – 8.44 \times 10^{-04}]$

FIGURE 5 Demographic history of the studied populations of *Podisma pedestris*, *P. carpetana*, and *P. cantabricae* inferred using STAIRWAY PLOT (only populations with ≥ 6 genotyped individuals were analyzed). Panels show the median of effective population size (N_e) over time, estimated assuming a mutation rate of 2.8×10^{-9} and 1-year generation time (both axes in a logarithmic scale). Vertical dashed line indicates the Last Glacial Maximum (LGM; ~21 ka BP). Population codes are described in Table S1.

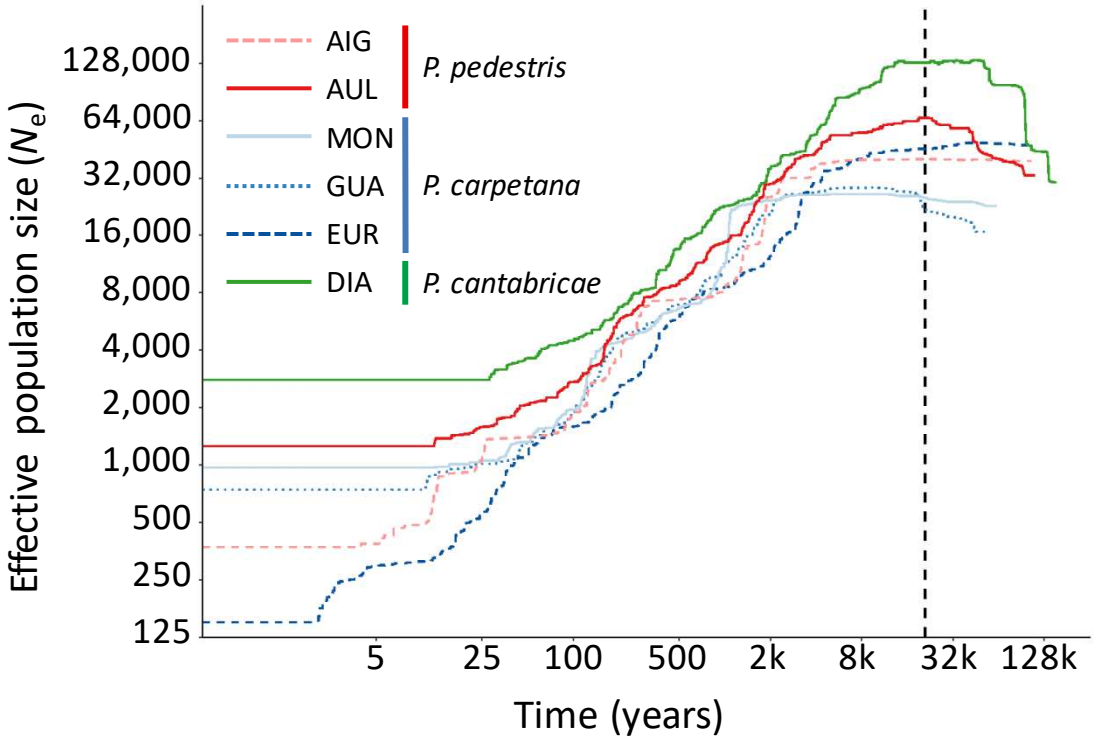

1323

1324

FIGURE 6 Current and last glacial maximum (LGM) distributions for each species as predicted by environmental niche models (ENM). Colors indicate areas predicted to be occupied by each species according to the maximum training sensitivity plus specificity (MTSS) logistic threshold of their respective ENM (Table S6). Predicted distributions for the LGM are based on the MIROC-ESM and the CCSM4 general atmospheric circulation models. Elevation shown by grey shading, with darker areas corresponding to higher elevations. Yellow color in current distribution maps indicate small areas (barely visible) predicted as suitable by ENMs but located outside the known distribution ranges of each species (i.e., over predictions). Current distribution maps show sampling localities (black dots with white rings) for each species; the small map inset shows the position of the species distribution on the Iberian Peninsula.

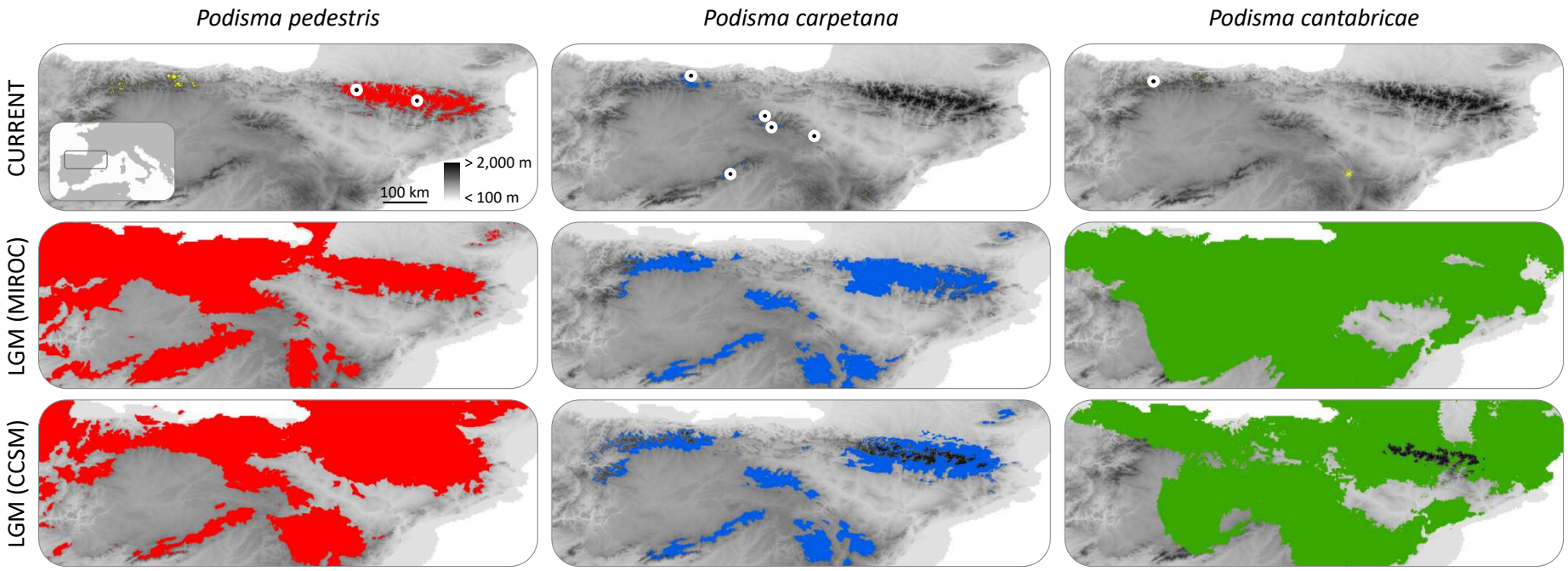

1333

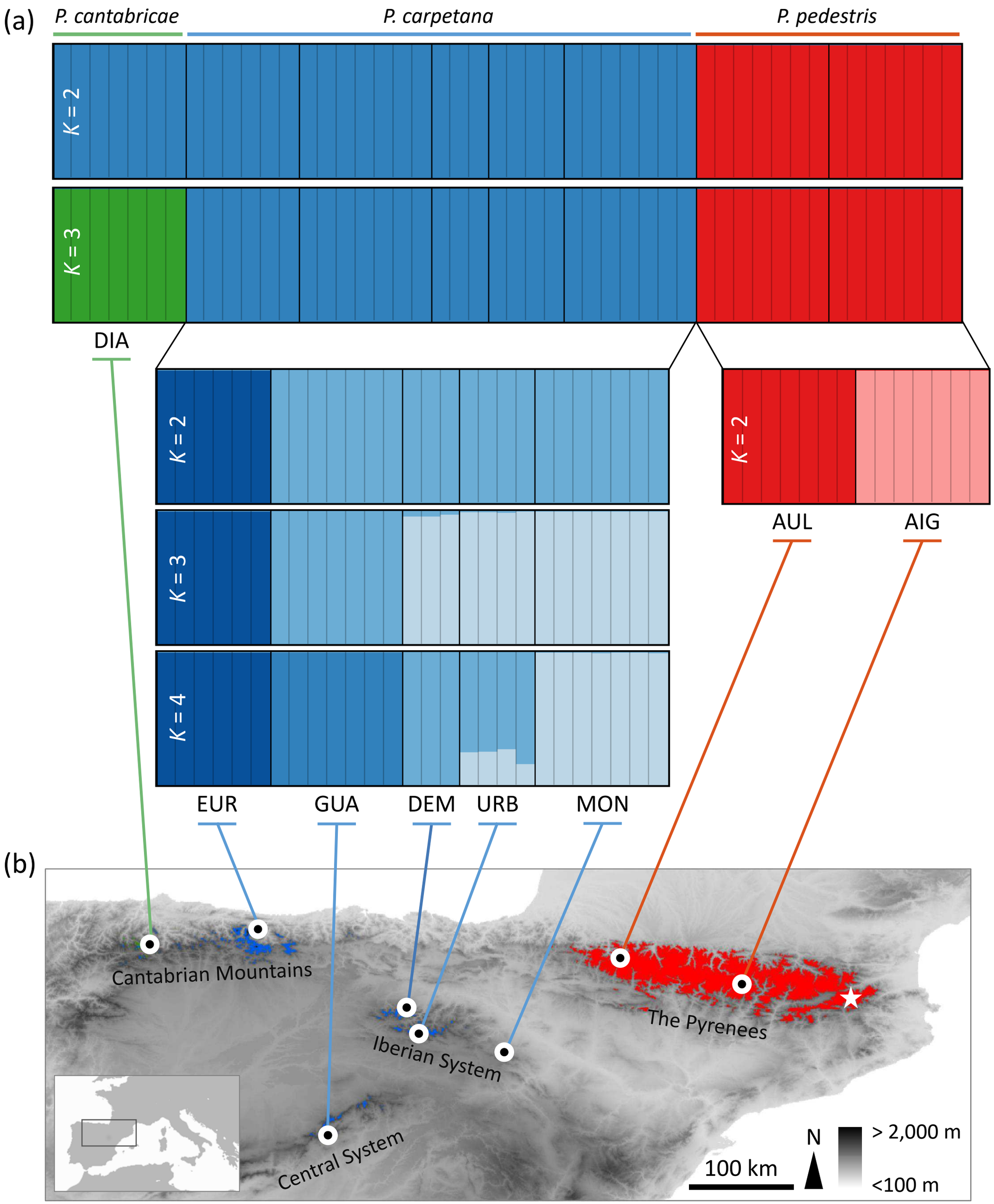

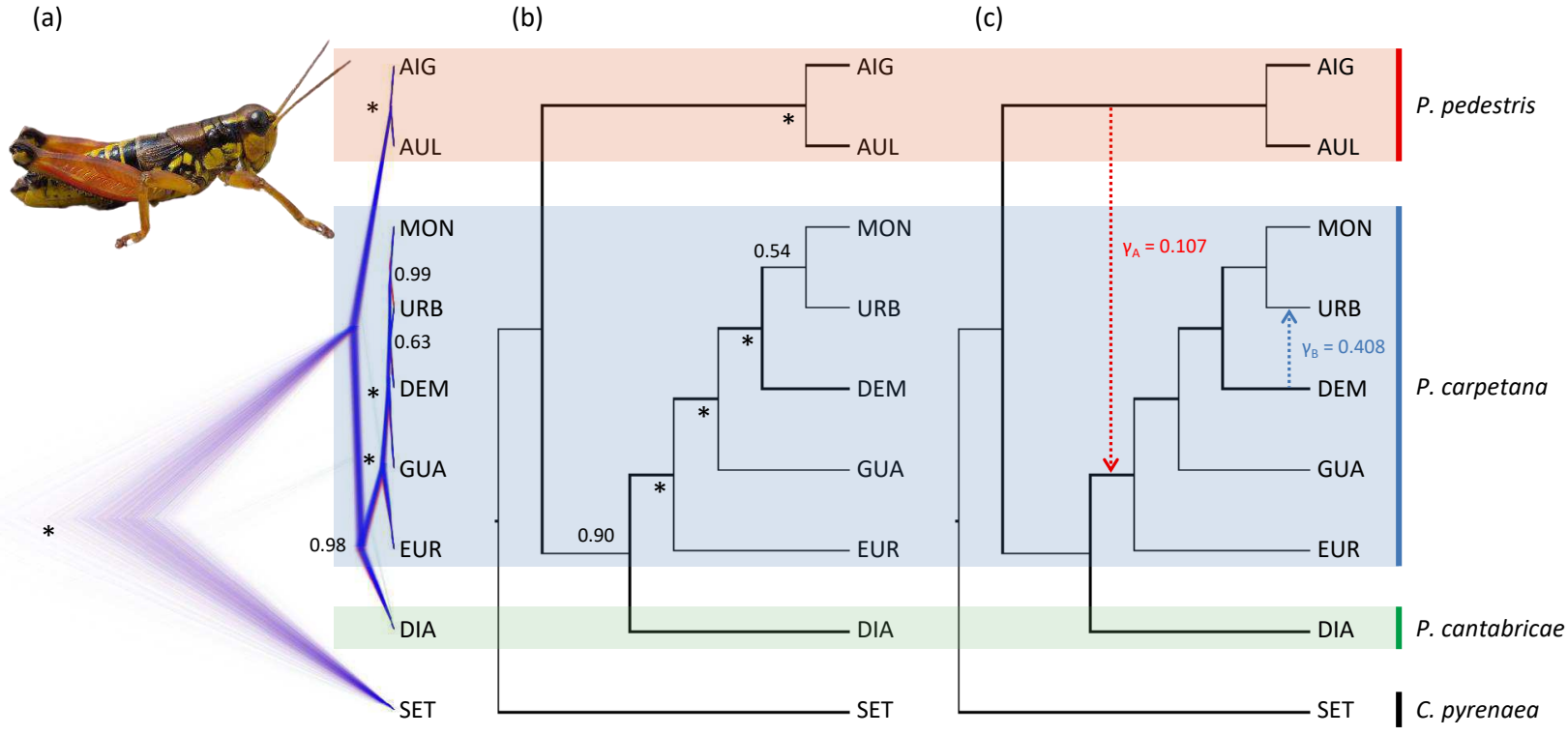

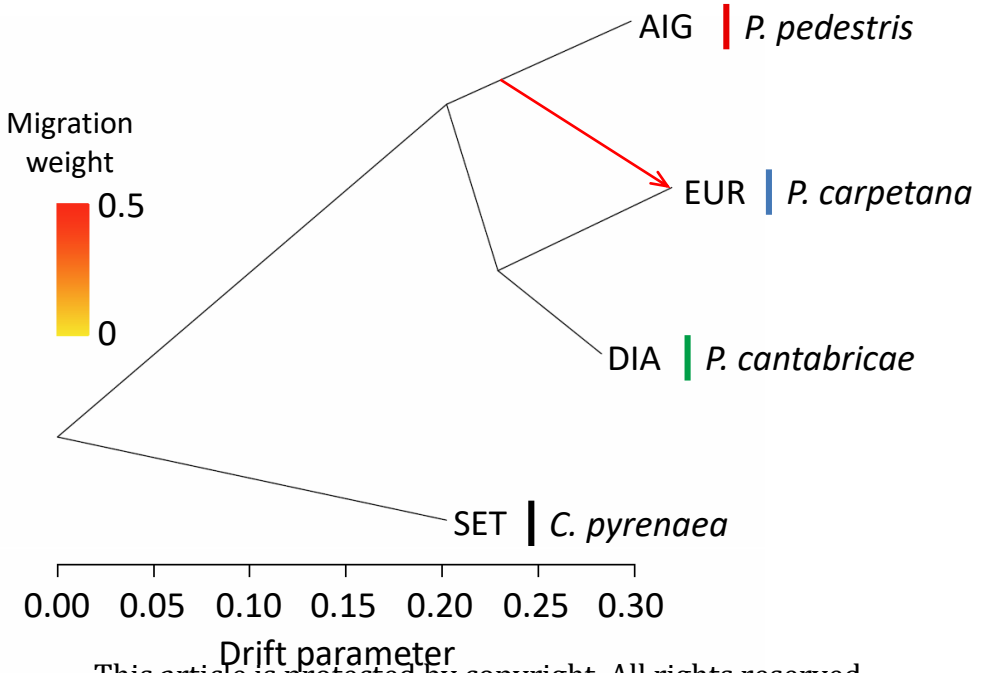

(a)

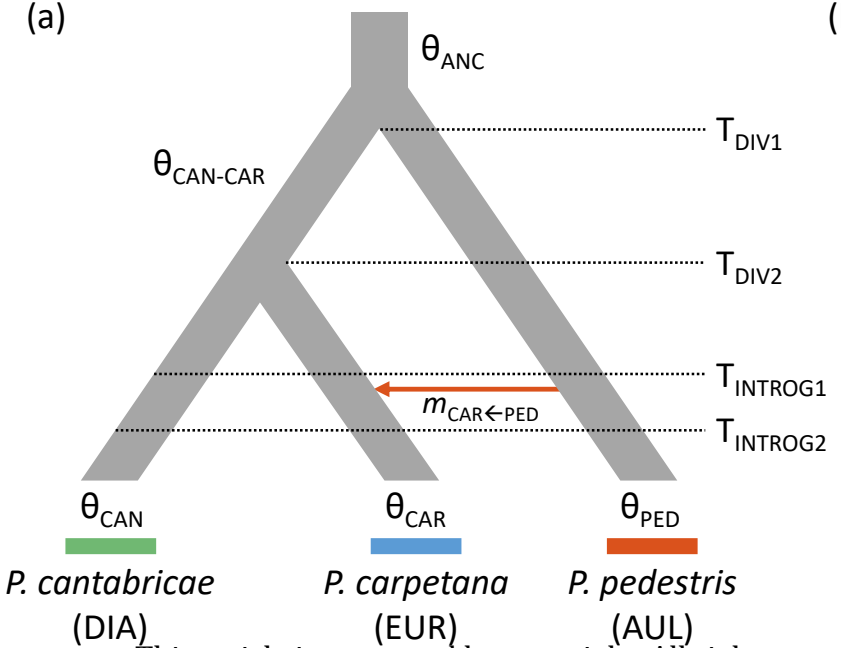

(b)

Parameter	Point estimate	95% CIs
θ_{ANC}	155,653	[29,151 – 418,990]
$\theta_{CAN\text{-}CAR}$	127,882	[47,710 – 194,084]
θ_{PED}	46,363	[39,453 – 55,707]
θ_{CAR}	64,394	[60,041 – 79,249]
θ_{CAN}*	71,429	-
T_{DIV1}	992,317	[178,271 – 1,086,881]
T_{DIV2}	135,537	[132,699 – 169,645]
$T_{INTROG1}$	108,047	[106,212 – 158,920]
$T_{INTROG2}$	104,545	[74,192 – 132,094]
$m_{CAR\leftarrow PED}$	7.75×10^{-04}	$[1.00 \times 10^{-05} – 8.44 \times 10^{-04}]$